FRIEDRICH-SCHILLER-UNIVERSITÄT JENA
PHYSIKALISCH-ASTRONOMISCHE-FAKULTÄT

FRIEDRICH-SCHILLER-
UNIVERSITÄT
JENA

SOMMERSEMESTER 2022

Fiber Optics

MARKUS SCHMIDT

LaTeX-Satz und Design von Martin Beyer

Contents

1 Motivation and Introduction

Books on Fiber Optics:

1. A. SNYDER, J. LOVE, "Optical Waveguide Theory", Springer Science & Business Media, 2012.
2. G. AGRAWAL, "Lightwave technology: telecommunication systems", John Wiley & Sons, 2005.
3. C. YEH, F. SHIMABUKURO, "The essence of dielectric waveguides", New York: Springer, 2008.

Fibers have two key properties which are relevant for waveguiding. The first is longitudinal invariance which allows for the propagation of light and the second is transverse confinement which leads to the formation of modes inside the fiber. The basic geometry of fibers consists of two parts - core and cladding - which are depicted in figure 1. Both parts differ in their optical properties, namely the refractive index.

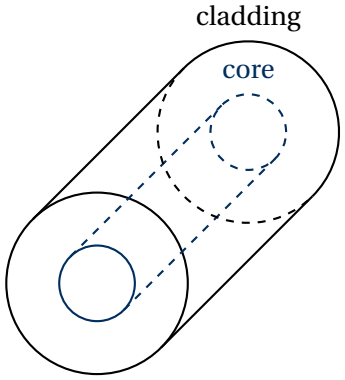

Figure 1: The two main components of an optical fiber.

The most prominent fiber to date is the *single mode fiber* SMF-28 which is used for telecommunication. It has a core diameter of 8 µm and a loss rate of 0,1 dB/km at a wavelength of $\lambda = 1{,}55\,\mu\text{m}$. This corresponds to a transmission of 50 % for a 30 km long fiber. Thus the typical lengths of such fibers are 10 km…100 km. Per annum more than 400 Million kilometers of fibers are fabricated. The majority of fibers are produced in China. The transmission capacity of a single cable is about $0{,}25 \cdot 10^{12}$ Letters/s. This corresponds to 62500 bibles per second. The field of fiber optics received a Nobel prize with CHARLES KAO in 2009. It was awarded for his discovery, that loss of information perceived in the 1960's is not an electronic problem, but rather comes from impurities. Thus the information loss is a chemical problem.

The main applications of fibers are:

- telecommunication
- endoscopy
- lasers/light sources (nonlinear optics)
- sensing (strain, stress, temperature)

Finally we want to mention statements about optical fibers. The first one is from B. Eggleton:

> "Bandwidth increases democracy."

Secondly we want to quote the National Academy of Engineering:

> "Fiber Optics is one of the greatest achievments in the 20th century."

2 Fundamentals

2.1 Modes in Waveguides

2.1.1 Example: Planar mirror waveguide

We want to start with an example of a very simple waveguide structure consisting of two metal parts separated by a dielectric layer. This is actually the only example where all equations can be solved analytically. Here we use some assumptions:

- No penetration into metal (perfect metal)
- Propagation along z-direction
- Invariance along y-direction.

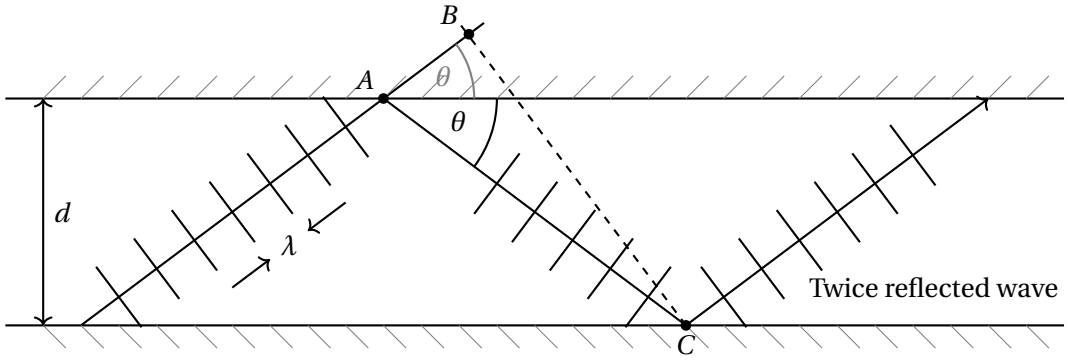

Figure 2: Geometry of the waveguide. For self consistency the wave has to duplicate itself after two reflections in the waveguide.

The geometry of the waveguide is displayed in figure 2. After two reflections the wave needs to duplicate thus we require the same phase of the waves at points B and C. If we note that the wave accumulates a phase shift of π at every reflection we find

$$k(\overline{AC} - \overline{AB}) - 2\pi = 2\pi q, \quad \text{with} \quad q \in \mathbb{N}. \tag{2.1}$$

Furthermore we find a geometric relation to describe $\overline{AC} - \overline{AB}$. First note that

$$\overline{AC} = \frac{d}{\sin\theta} \quad \text{and} \quad \cos(2\theta) = 1 - 2\sin^2\theta = \frac{\overline{AB}}{\overline{AC}} \Rightarrow \overline{AB} = \overline{AC}(1 - 2\sin^2\theta). \tag{2.2}$$

Then we find

$$\begin{aligned} \overline{AC} - \overline{AB} &= 2\sin^2\theta\,\overline{AC} = 2d\sin\theta \\ \Rightarrow k(\overline{AC} - \overline{AB}) &= 2dk\sin\theta = m2\pi \quad \text{with} \quad m = 1,2,3,\ldots. \end{aligned} \tag{2.3}$$

This leads to a discretization of angles with

$$\sin\theta = m\frac{\pi}{dk} = m\frac{\lambda_0}{2dn} \quad \Rightarrow \quad \theta_m = \arcsin\left(m\frac{\lambda_0}{2dn}\right). \tag{2.4}$$

This formula correlates the discrete angles with the wavelength. For the case of $d \gg \lambda_0$ the angles are small and can be approximated by

$$\theta_m \approx m\frac{\lambda_0}{2dn}. \tag{2.5}$$

We observe that modes of higher orders have larger angles.

Now we want to describe the field of the modes. We start by decomposing the wave vector into longitudinal and transverse vector components as shown in figure 3. For translational invariant modes one ray is not enough to describe the field but rather we need to superimpose two oppositely zigzagging rays:

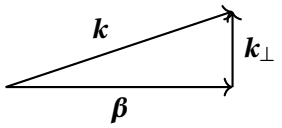

Figure 3: Wave vector diagram.

$$\begin{aligned} A_1(x,z) &= A_m e^{ik_\perp x} e^{i\beta z} \\ A_2(x,z) &= A_m e^{-ik_\perp x} e^{i\beta z}, \end{aligned} \tag{2.6}$$

where A_m is the amplitude, $e^{\pm ik_\perp x}$ the transverse phase and $e^{i\beta z}$ the longitudinal phase. Adding both rays results in

$$A = A_1 \pm A_2 = A_m e^{i\beta z}(e^{ik_\perp x} \pm e^{-ik_\perp x}) = 2A_m e^{i\beta z} \begin{cases} \cos(k_\perp x) & \text{“+”} \\ i\sin(k_\perp x) & \text{“−”} \end{cases} \tag{2.7}$$

$$\Rightarrow \boxed{A = 2A_m e^{i\beta z} u(z)} \quad \text{General form a mode.} \tag{2.8}$$

Here $u(z)$ is a function describing the transverse mode pattern. The amplitude A_m is important for normalization.

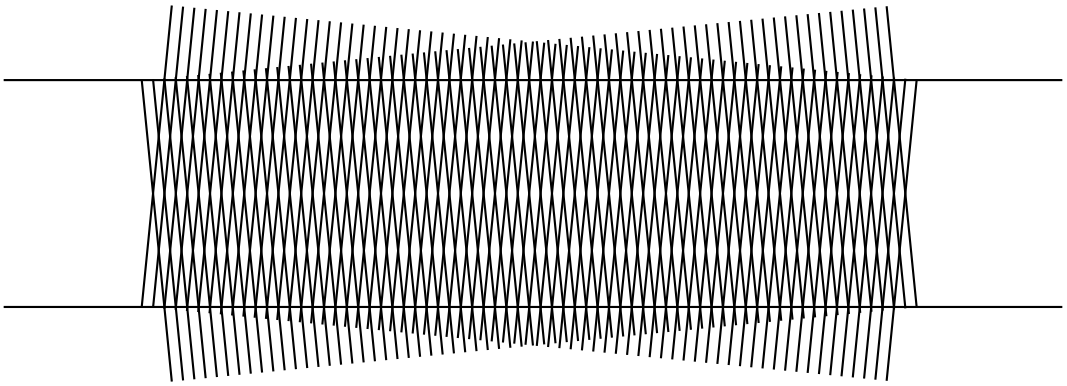

Figure 4: At angles for which self-consistency is satisfied, the two waves interfere and create a pattern that does not change with z. The shown example is a mode of order $m = 4$.

The key for the waveguide is the *phase factor* β. It can be expressed by the the $\boldsymbol{k}$-vector and the transverse wave vector $k_\perp$ which is given as

$$k_\perp = \sin\theta_m k \overset{(2.4)}{=} m\frac{\pi}{d}. \tag{2.9}$$

Then with $k^2 = \beta^2 + k_\perp^2$ we can write β as

$$\beta = \sqrt{k^2 - k_\perp^2} = \sqrt{\left(n\frac{2\pi}{\lambda_0}\right)^2 - \left(\frac{m\pi}{d}\right)^2} = nk_0 \underbrace{\sqrt{1 - \left(\frac{m\pi}{nk_0 d}\right)^2}}_{\text{Modification by confinement}} . \tag{2.10}$$

Now we can define a refractive index via $\beta = n_{\text{eff}} k_0$

$$\boxed{n_{\text{eff}} = n\sqrt{1 - \left(\frac{m\pi}{nk_0 d}\right)^2}}. \tag{2.11}$$

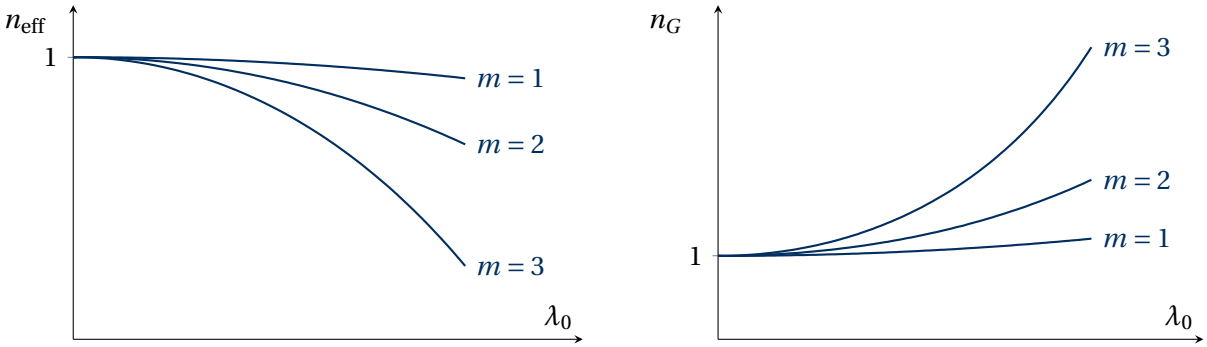

Figure 5: Left: effective index of a mirror waveguide as a function of λ_0. For higher order modes the index changes more rapidly for higher wavelengths.
Right: Group index of a mirror waveguides for different modes.

This is also called the *dispersion equation of a mirror waveguide.*

The phase of the mode is $\Phi = \exp(\mathrm{i} n_{\text{eff}} k_0 z)$. If we let $d \to \infty$ we will have $n = n_{\text{eff}}$ in the limit and Φ corresponds to a plane wave. Therefore the confinement of the wave has an impact on the phase and is very import.

Let us now revise some familiar quantities. First we state what phase and group velocity are:

$$v_p = \frac{\omega}{\beta} \quad \text{phase velocity} \tag{2.12}$$

$$v_G = \frac{\partial \omega}{\partial \beta} \quad \text{group velocity.} \tag{2.13}$$

The phase velocity describes the speed of the wavefronts. For a plane wave we find $v_p = \frac{c_0}{n} \leq c_0$ that the speed is always smaller than the speed of light. For waveguide modes, however, the phase velocity

$$v_p = \frac{2\pi\nu_0}{n_{\text{eff}} k_0} = \frac{c_0}{n_{\text{eff}}} \geq c_0 \tag{2.14}$$

is larger than one whereas the group velocity

$$v_G = \frac{c_0}{n} \underbrace{\sqrt{1 - \left(\frac{m\pi}{nk_0 d}\right)^2}}_{\text{confinement}} = \frac{c_0}{n^2} n_{\text{eff}} < c_0 \tag{2.15}$$

is always smaller than the speed of light. Using the group velocity we can also introduce a quantity called the *group index* given as

$$n_G = \frac{c_0}{v_G} = \frac{n^2}{n_{\text{eff}}}. \tag{2.16}$$

Finally we want to write down the electromagnetic field of a mirror waveguide for TE-polarization

$$E_y(x,z) = C u_m(x) \mathrm{e}^{\mathrm{i}\beta z} \quad \text{with} \quad u_m(x) = \begin{cases} \cos(k_\perp x) \\ \mathrm{i}\sin(k_\perp x). \end{cases} \tag{2.17}$$

Using the boundary condition at the metal plates with $E_y(x = \pm\frac{d}{2}) = 0$ we find

$$u_m(x) = \begin{cases} \cos\left(\frac{m\pi}{d}x\right) & m = 1,3,5,\ldots \\ \mathrm{i}\sin\left(\frac{m\pi}{d}x\right) & m = 2,4,6,\ldots \end{cases}. \tag{2.18}$$

The amplitude C can be calculated via a normalization condition

$$1 \stackrel{!}{=} \left| \int_{-\infty}^{\infty} |E_y|^2 \,\mathrm{d}x \right| = \int_{-d/2}^{d/2} C^2 u_m^2(x) \,\mathrm{d}x \quad \Rightarrow \quad C = \sqrt{\frac{2}{d}}. \tag{2.19}$$

Using these conditions the total electric field of a mirrored waveguide is

$$\boxed{E_y(x,z) = \sqrt{\frac{2}{d}} \mathrm{e}^{\mathrm{i}\beta z} \begin{cases} \cos\left(\frac{m\pi}{d}x\right) & m = 1,3,5,\ldots \quad \text{even modes} \\ \mathrm{i}\sin\left(\frac{m\pi}{d}x\right) & m = 2,4,6,\ldots \quad \text{odd modes} \end{cases}} \tag{2.20}$$

The number of allowed modes is given by the condition

$$\sin\theta_m = m\frac{\lambda_0}{2dn} \leq 1 \quad \Rightarrow m = \left\lfloor 2n\frac{d}{\lambda_0} \right\rfloor. \tag{2.21}$$

Then we find the condition for single mode operation as

$$\lambda_{SM} = n \cdot d < \lambda_0 < \lambda_C = 2nd \quad \text{or} \quad d < \frac{\lambda_0}{n} < 2d, \tag{2.22}$$

where λ_{SM} is the single mode wavelength and λ_C the cut-off wavelength for all modes.

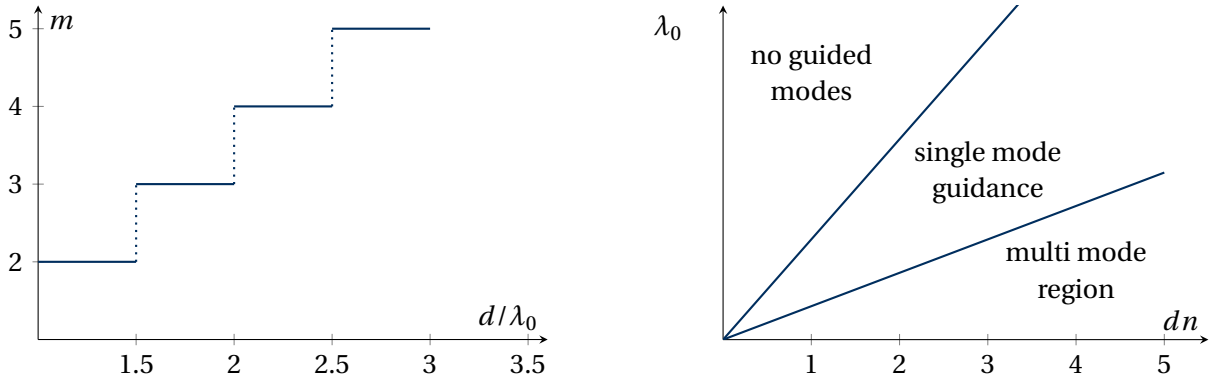

Figure 6: Left: Number of allowed modes as a function of d/λ_0.
Right: Regions for single-mode guidance, multi-mode guidance or no guided modes.

2.1.2 Fundamental properties of modes (lossless)

So far we have only talked about guided modes as any waveguide supports a discrete number of bounded modes. However, for external radiation on the side of the waveguide allows for the propagation of a continuum of radiation modes as well.

Total electric field

Due to the linearity of Maxwells equations the total electric field can now be written as

$$\boldsymbol{E}_{\text{tot}}(x,y,z) = \underbrace{\sum_j a_j \boldsymbol{E}_j^{\beta}(x,y,z)}_{\text{forward}} + \underbrace{\sum_j a_{-j} \boldsymbol{E}_j^{\beta}(x,y,z)}_{\text{backward}} + \boldsymbol{E}_{\text{rad}}, \tag{2.23}$$

where a_j are the modal amplitudes which depend on the excitation of the modes. The bounded modes $\boldsymbol{E}_j^{\beta}(x,y,z)$ can be written as

$$\boldsymbol{E}_j^{\beta}(x,y,z) = \boldsymbol{E}_j(x,y)\mathrm{e}^{\mathrm{i}\beta_j z} = \big[\underbrace{\boldsymbol{E}_j^{\perp}(x,y)}_{\text{transverse}} + \underbrace{E_{j,z}(x,y)\hat{\mathbf{e}}_z}_{\text{longitudinal}}\big]\mathrm{e}^{\mathrm{i}\beta_j z}. \tag{2.24}$$

Orthogonality and normalization

Regarding orthogonality and normalization of the fields we can make use of the reciprocity theorem

$$\int_{A_\infty} (\boldsymbol{E}_j \times \boldsymbol{H}_k^*)_z \,\mathrm{d}A = 0 \quad \text{for} \quad j \neq k. \tag{2.25}$$

Then the normalization constants are given by

$$N_j = \frac{1}{2}\left|\int_{A_\infty} (\boldsymbol{E}_j \times \boldsymbol{H}_j^*)_z \,\mathrm{d}A\right| \quad \Rightarrow \boldsymbol{E}_j^N = \frac{1}{\sqrt{N_j}}\boldsymbol{E}_j, \boldsymbol{H}_j^N = \frac{1}{\sqrt{N_j}}\boldsymbol{H}_j. \tag{2.26}$$

Then the find the following relation

$$\boxed{\frac{1}{2}\int_{A_\infty}(\boldsymbol{E}_j^N \times \boldsymbol{H}_k^N)_z \,\mathrm{d}A = \delta_{jk}} \tag{2.27}$$

Power in modes

The power density in the modes is given by the Poynting vector

$$S_j = \frac{1}{2}|a_j|^2 \,\mathrm{Re}(\boldsymbol{E}_j^B \times \boldsymbol{H}_j^{B*})_z = \frac{1}{2}|a_j|^2 (\boldsymbol{E}_j \times \boldsymbol{H}_j^*)_z. \tag{2.28}$$

Then the total power of one mode is given by the integral over the power density

$$P_j = \int_{A_\infty} S_j \,\mathrm{d}A = \frac{1}{2}|a|_j^2 \int_{A_\infty} (\boldsymbol{E}_j \times \boldsymbol{H}_j^*)_z \,\mathrm{d}A = |a_j|^2 N_j. \tag{2.29}$$

We observe that the power depends on the modal amplitudes.
In the following we want to discuss a procedure on how to obtain the amplitudes a_j:

1. Take the vector product with $\boldsymbol{H}_j^{N*}$.
2. Use the orthogonality theorem.

$$\begin{aligned}
\boldsymbol{E}_I^N \times \boldsymbol{H}_1^{N*} &= a_1 \boldsymbol{E}_1^N \times \boldsymbol{H}_1^{N*} + a_2 \boldsymbol{E}_2^N \times \boldsymbol{H}_1^N \\
\int_{A_\infty} (\boldsymbol{E}_I^N \times \boldsymbol{H}_1^{N*}) \,\mathrm{d}A &= a_1 \underbrace{\int_{A_\infty} (\boldsymbol{E}_1^N \times \boldsymbol{H}_1^{N*}) \,\mathrm{d}A}_{=2} + a_2 \underbrace{\int_{A_\infty} (\boldsymbol{E}_2^N \times \boldsymbol{H}_1^{N*}) \,\mathrm{d}A}_{=0} \\
\Rightarrow a_1 &= \frac{1}{2}\int_{A_\infty} (\boldsymbol{E}_I^N \times \boldsymbol{H}_1^{N*}) \,\mathrm{d}A.
\end{aligned} \tag{2.30}$$

We find that the amplitude of the 1st mode is given by the overlap integral between input field and mode 1. In a case that mode 1 has a similar pattern to the input mode we find $a_1 \gg a_2$ and thus $P_1 \gg P_2$. Therefore we observe a strong excitation of mode 1.

The total power is given by the sum of the modal powers and thus depends on the modal amplitudes

$$P_{\mathrm{tot}} = \sum_j P_j = \sum_j |a_j|^2 + (P_{\mathrm{RAD}}). \tag{2.31}$$

Many applications require as-high-as possible power in the fundamental mode. Therefore the optimization of the coupling is crucial.

Modes in step-index Waveguides

In the following we want to distinguish between planar slab waveguides and cylindrical fibers. We call ρ the waveguide extension

$$\rho = \begin{cases} \frac{d}{2} & \text{planar WG} \\ R & \text{Fiber WG} \end{cases}. \tag{2.32}$$

Using this we also want to define the *waveguide parameter* V as

$$V = 2\pi \frac{\rho}{\lambda_0} \sqrt{n_{\text{Co}}^2 - n_{\text{Cl}}^2}. \tag{2.33}$$

It allows to define the domain of single-mode operation ($V \approx 1$). For $V \gg 1$ we are in the Multi-Mode operation regime.

Furthermore we want to define two *modal parameters*

$$\begin{aligned} U &= \rho \sqrt{k_0^2 n_{\text{Co}}^2 - \beta^2} \quad \text{Core}, \\ W &= \rho \sqrt{\beta^2 - k_0^2 n_{\text{Cl}}^2} \quad \text{Cladding}. \end{aligned} \tag{2.34}$$

For guided modes in non-absorbing waveguides both parameters are real valued.
Step-index-waveguides operate by total internal reflection at the interface between core and cladding. For this the waveguide has to satisfy the following condition:

$$\boxed{n_{\text{Core}} > n_{\text{Cladding}}}. \tag{2.35}$$

In order to form bounded Modes a waveguides effective index must lie in between the refractive index of core and cladding

$$\boxed{n_{\text{Cl}} < n_{\text{eff}} < n_{\text{Core}}}. \tag{2.36}$$

Using these conditions we can formulate boundaries and relations between the modal parameters

$$0 \leq U < V, \quad 0 \leq W < V, \quad V^2 = U^2 + W^2. \tag{2.37}$$

Finally we want to define cut-off point when $\beta = n_{\text{Cl}} k_0$ which leads to $U = V$ and thus $W = 0$. In this case the Modes are highly delocalized.

Procedure to find modes in WG

Solving Maxwells equations for core and cladding yields

$$(\nabla_t^2 + n_{\text{Co}}^2 k_0^2 - \beta^2) E_z(x, y) = 0 \tag{2.38}$$

$$(\nabla_t^2 + n_{\text{Cl}}^2 k_0^2 - \beta^2) E_z(x, y) = 0, \tag{2.39}$$

where ∇_t^2 is the transverse Laplace Operator and $E_z(x, y)$ the longitudinal field. The procedure to find the modes is now:

1. Find functions that solve the two wave equations independently.
2. Apply boundary conditions at the core/cladding interface. This yields a dispersion equation $\beta = \beta(\lambda_0)$.
3. Calculate the modes.

2.1.3 Modes in fibers

We now want to model a simple fiber with a core of refractive index n_1, extension ρ, a cladding with n_2 and an infinite extension. Our goal is to analyze the dispersion relation, number of modes and the mode pattern.

Step 1: Maxwells equations in cylindrical coordinates.

As a simplification we only consider forward propagation modes and no radiation modes. Then the electric and magnetic field of the bounded modes are given by

$$\boldsymbol{E}^B(r,\varphi,z) = \boldsymbol{E}(r,\varphi)\mathrm{e}^{\mathrm{i}\beta z}\mathrm{e}^{-\mathrm{i}\omega t}, \qquad \boldsymbol{H}^B(r,\varphi,z) = \boldsymbol{H}(r,\varphi)\mathrm{e}^{\mathrm{i}\beta z}\mathrm{e}^{-\mathrm{i}\omega t}. \tag{2.40}$$

Now using Maxwells equations we find

$$\begin{aligned} \vec{\nabla}\times\boldsymbol{H}^B = \partial t\boldsymbol{D}^B = -\mathrm{i}\omega\varepsilon\varepsilon_0\boldsymbol{E}^B \quad &\Rightarrow \quad \vec{\nabla}\times\boldsymbol{H} = -\mathrm{i}\omega\varepsilon\varepsilon_0\boldsymbol{E} \\ \vec{\nabla}\times\boldsymbol{E}^B = -\mu_0\partial t\boldsymbol{H}^B = -\mathrm{i}\omega\mu_0\boldsymbol{H}^B \quad &\Rightarrow \quad \vec{\nabla}\times\boldsymbol{E} = \mathrm{i}\omega\mu_0\boldsymbol{H}. \end{aligned} \tag{2.41}$$

It can be shown that the transverse components depend on the longitudinal components $E_\varphi = E_\varphi(E_z, H_z)$. Then the transverse components are given by

$$\begin{aligned} E_\varphi &= -K\left(-\frac{n_{\text{eff}}}{r}\frac{\partial}{\partial\varphi}E_z + \frac{1}{\varepsilon_0 c_0}\frac{\partial}{\partial r}H_z\right) \\ H_\varphi &= K\left(\frac{n_{\text{eff}}}{r}\frac{\partial}{\partial\varphi}H_z + \varepsilon_0 c_0\varepsilon\frac{\partial}{\partial r}E_z\right) \\ E_r &= K\left(n_{\text{eff}}\frac{\partial}{\partial r}E_z + \frac{1}{\varepsilon_0 c_0 r}\frac{\partial}{\partial\varphi}H_z\right) \\ H_r &= K\left(n_{\text{eff}}\frac{\partial}{\partial r}H_z - \frac{\varepsilon\varepsilon_0 c_0}{r}\frac{\partial}{\partial\varphi}E_z\right) \quad \text{with} \quad K = \frac{\mathrm{i}}{k_0(\varepsilon - n_{\text{eff}}^2)}. \end{aligned} \tag{2.42}$$

Step 2: Derive the differential equation

For the longitudinal fields we can now derive a differential equation for magnetic and electric field

$$\vec{\nabla}\times\left(\vec{\nabla}\times\boldsymbol{H}\right) = \vec{\nabla}\underbrace{(\vec{\nabla}\cdot\boldsymbol{H})}_{=0} - \Delta\boldsymbol{H} = -\mathrm{i}\omega\varepsilon\varepsilon_0\underbrace{\vec{\nabla}\times\boldsymbol{E}}_{\mathrm{i}\omega\mu_0\boldsymbol{H}} = \varepsilon\frac{\omega^2}{c_0^2}\boldsymbol{H}, \tag{2.43}$$

$$\vec{\nabla}\times\left(\vec{\nabla}\times\boldsymbol{E}\right) = \vec{\nabla}\underbrace{(\vec{\nabla}\cdot\boldsymbol{E})}_{=0} - \Delta\boldsymbol{E} = \mathrm{i}\omega\mu_0\underbrace{\vec{\nabla}\times\boldsymbol{H}}_{-\mathrm{i}\omega\varepsilon\varepsilon_0\boldsymbol{E}} = \varepsilon\frac{\omega^2}{c_0^2}\boldsymbol{E}. \tag{2.44}$$

We can generalize this to the following field equation

$$\Delta\Psi_s + \varepsilon k_0^2\Psi_s = 0 \quad \text{with} \quad \Delta = \frac{\partial^2}{\partial r^2} + \frac{1}{r}\frac{\partial}{\partial r} + \frac{1}{r^2}\frac{\partial^2}{\partial\varphi^2} + \frac{\partial^2}{\partial z^2}. \tag{2.45}$$

For the solution we make the ansatz

$$\Psi_s = \Psi(r,\varphi)e^{i\beta z} \quad \Rightarrow \quad \left(\frac{\partial^2}{\partial r^2} + \frac{1}{r}\frac{\partial}{\partial r} + \frac{1}{r^2}\frac{\partial^2}{\partial \varphi^2} + \varepsilon k_0^2 - \beta^2\right)\Psi = 0. \tag{2.46}$$

Let us define a *normalized radial component* as

$$R := \frac{r}{\varrho} \Rightarrow \begin{cases} 0 \le R \le 1 & \text{Core} \\ 1 < R < \infty & \text{Cladding} \end{cases}. \tag{2.47}$$

Then the differential equation transforms to

$$\left(\frac{\partial^2}{\partial R^2} + \frac{1}{R}\frac{\partial}{\partial R} + \frac{1}{R^2}\frac{\partial^2}{\partial \varphi^2} + \varrho(\varepsilon k_0^2 - \beta^2)\right)\Psi = 0. \tag{2.48}$$

We can obtain separable solutions for

$$\Psi \sim \begin{cases} \cos(m\varphi) \\ \sin(m\varphi) \end{cases} \qquad \text{with} \quad m = 0,1,2,\ldots \tag{2.49}$$

Now using the modal parameters we can use this ansatz to write down the differential equation for core and cladding

$$\left(\frac{\partial^2}{\partial R^2} + \frac{1}{R}\frac{\partial}{\partial R} + U^2 - \left(\frac{m}{R}\right)^2\right)\Psi = 0 \quad \text{Bessel differential equation} \tag{2.50}$$

$$\left(\frac{\partial^2}{\partial R^2} + \frac{1}{R}\frac{\partial}{\partial R} - W^2 - \left(\frac{m}{R}\right)^2\right)\Psi = 0 \quad \text{Modified Bessel differential equation} \tag{2.51}$$

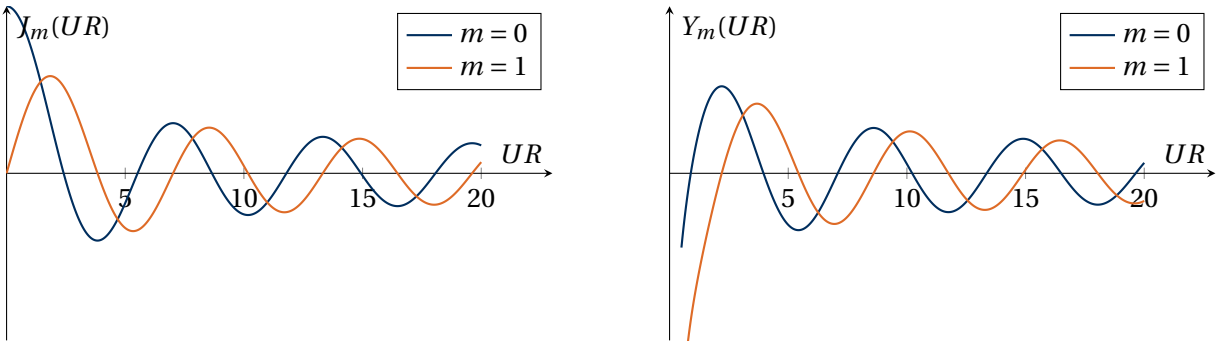

Figure 7: Two possible solutions of the Bessel differential equation (2.50). For $U \to 0$ we find $Y_m(UR) \to -\infty$. However, the modes are finite at $R = 0$. Therefore we need to drop the Y_m solutions. Thus the solutions in the core have the form $J_m(UR)$.

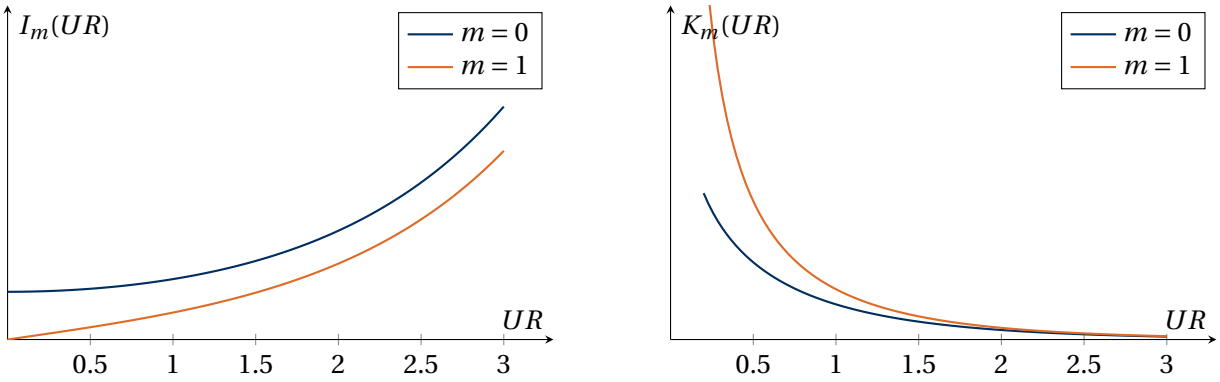

Figure 8: Two possible solutions of the modified Bessel differential equation (2.51). For $W \to \infty$ we find $I_m(UR) \to \infty$. However, the modes ought to have no fields at $R \to \infty$. Therefore we need to drop the I_m solutions. Thus the solutions in the cladding have the form $K_m(UR)$.

In the following table we want to list the ansatz functions for the longitudinal fields E_z and H_z.

Table 1: Ansatz functions for the longitudinal fields

	E_z	H_z	function type
core	$A\frac{J_m(UR)}{J_m(U)} f_m(\varphi)$	$B\frac{J_m(UR)}{J_m(U)} g_m(\varphi)$	Oscillating, sinus-type
cladding	$A\frac{K_m(WR)}{K_m(W)} f_m(\varphi)$	$B\frac{K_m(WR)}{K_m(W)} g_m(\varphi)$	decaying, exponential-type

At the cut-off we find $n_{\text{eff}} = n_2$. This means

$$\begin{aligned} U = V \quad &\Rightarrow \quad \frac{J_m(UR)}{J_m(U)} = \frac{J_m(VR)}{J_m(V)} \\ W = 0 \quad &\Rightarrow \quad \frac{K_m(WR)}{K_m(W)} \quad \text{slow decay.} \end{aligned} \tag{2.52}$$

Close to the cut-off, the modes get delocalized.

Now we want to define the *boundary coefficients* A, B which are to be determined by the boundary conditions of the azimuthal field components. For the azimuthal factors $f_m(\varphi)$ and $g_m(\varphi)$ we choose

$$\left.\begin{aligned} f_m(\varphi) &= \cos(m\varphi) \\ g_m(\varphi) &= \sin(m\varphi) \end{aligned}\right\} \quad \text{leads to even modes} \quad . \tag{2.53}$$

Step 3: Find dispersion relation from the boundary conditions

First we want to state the continuity condition of the parallel component of electric and magnetic field. We start by integrating over Maxwells equation and using Stokes theorem

$$\int_S \vec{\nabla} \times \boldsymbol{E}\,\mathrm{d}\boldsymbol{s} = \oint_{\partial S} \boldsymbol{E}\,\mathrm{d}\boldsymbol{r} = -\frac{\partial}{\partial t}\underbrace{\int_S \boldsymbol{B}\,\mathrm{d}\boldsymbol{s}}_{=0}$$

$$\Rightarrow \boldsymbol{n}_1 \times (\boldsymbol{E}_1 - \boldsymbol{E}_2) = 0 \quad \Rightarrow \quad \boxed{E_1^{\parallel} = E_2^{\parallel}}. \tag{2.54}$$

The electric field component parallel to the boundary surface is continuous. The magnetic component is calculated analogously

$$\int_S \vec{\nabla} \times \boldsymbol{H}\,\mathrm{d}\boldsymbol{s} = \oint_{\partial S} \boldsymbol{H}\,\mathrm{d}\boldsymbol{r} = \int_S \boldsymbol{j}\,\mathrm{d}\boldsymbol{s} + \frac{\partial}{\partial t}\underbrace{\int_S \boldsymbol{D}\,\mathrm{d}\boldsymbol{s}}_{=0}$$

$$\Rightarrow \boldsymbol{n}_1 \times (\boldsymbol{H}_1 - \boldsymbol{H}_2) = \boldsymbol{K} \quad \Rightarrow \quad \boxed{H_1^{\parallel} = H_2^{\parallel}} \quad \text{for} \quad K = 0. \tag{2.55}$$

Here K describes a macroscopic surface current, however, at optical frequencies no macroscopic current can be measured. Therefore, both fields are continuous across the boundary.

We now want to consider the boundary conditions for a step index fiber. We can formulate four conditions ar $r = \varrho, R = 1$:

$$\begin{aligned} &\text{BC1: } E_z^1 = E_z^2 \qquad \text{BC2: } H_z^1 = H_z^2 \\ &\text{BC3: } E_\varphi^1 = E_\varphi^2 \qquad \text{BC4: } H_\varphi^1 = H_\varphi^2. \end{aligned} \tag{2.56}$$

We observe that BC1 and BC2 are automatically fulfilled by our ansatz in table 1

$$\begin{aligned} &\text{BC1: } A\frac{J_m(UR)}{J_m(U)}\bigg|_{R=1} f_m(\varphi) = A\frac{K_m(WR)}{K_m(W)}\bigg|_{R=1} f_m(\varphi) \\ &\text{BC2: } B\frac{J_m(UR)}{J_m(U)}\bigg|_{R=1} g_m(\varphi) = B\frac{K_m(WR)}{K_m(W)}\bigg|_{R=1} g_m(\varphi). \end{aligned} \tag{2.57}$$

Since only the ratio A/B is important we can set $B = 1$. In order to find the corresponding dispersion equation we have to

- use BC3 and solve for A_{BC3}
- use BC4 and solve for A_{BC4}
- Set $A_{\mathrm{BC3}} = A_{\mathrm{BC4}}$.

Dispersion equation of modes in cylindrical step-index fibers

$$\underbrace{\left[\frac{J_m'(U)}{UJ_m(U)} + \frac{K_m'(W)}{WK_m(W)}\right]}_{f_{\mathrm{TE}}}\underbrace{\left[\frac{J_m'(U)}{UJ_m(U)} + \left(\frac{n_2}{n_1}\right)^2\frac{K_m'(W)}{WK_m(W)}\right]}_{f_{\mathrm{TM}}} = \underbrace{\left(\frac{m\beta}{k_0 n_1}\right)^2\left(\frac{V}{UW}\right)^4}_{f_c} \tag{2.58}$$

We want to state some properties of equation (2.58)

- It is a transcendental equation. It has to be solved numerically

- For $m = 0$ the equation simplifies because $f_c = 0$ to

$$f_{\mathrm{TE}} f_{\mathrm{TM}} = 0 \quad \begin{cases} \text{TE modes for } f_{\mathrm{TE}} = 0 \\ \text{TM modes for } f_{\mathrm{TM}} = 0. \end{cases} \tag{2.59}$$

- It can also be applied for lossy materials by the implementation of complex root finders.

We now want to discuss the properties of the TE-solutions. The equation we need to solve is

$$\frac{J_0'(U)}{UJ_0(U)} = -\frac{K_0'(W)}{WK_0(W)} \quad \text{with} \quad f_{\mathrm{TE}} = 0. \tag{2.60}$$

Now using the relations $K_0'(x) = -K_1(x)$ and $J_0'(x) = -J_1(x)$ we find

$$\underbrace{\frac{J_1(U)}{UJ_0(U)}}_{f_{\mathrm{TE}}^L} = \underbrace{-\frac{K_1(W)}{WK_0(W)}}_{f_{\mathrm{TE}}^R}. \tag{2.61}$$

In order to find solutions we plot both functions and look for intersections (figure 9).

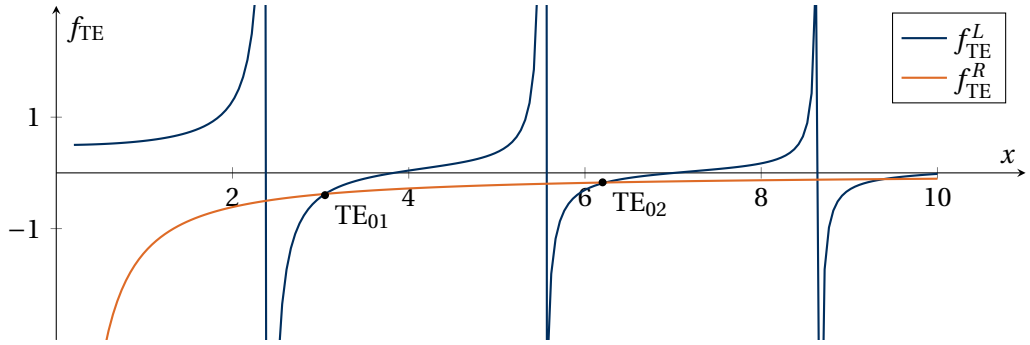

Figure 9: Graphical solution of equation (2.61). The nomenclature of the TE$_{mn}$ modes is as follows: m describes the order of the Bessel function while n is the order of the root. We distinguish between the dominant polarization with TE or TM.

We now want to list all possible modes in a fiber:

- TE: $E_z, E_r, H_\varphi = 0$, E_φ dominant
- TM: $E_\varphi, H_r, H_z = 0$, H_φ dominant
- EH: E_φ dominant, HE: H_φ dominant.

The EH and HE modes are called *hybrid modes* because all six components of the electric and magnetic field are in general nonzero.

Furthermore we can show that HE$_{11}$-mode exists for any ratio of ϱ/λ_0, therefore we call it the fundamental fiber mode. The single mode condition of a fiber is given by

$$V = \frac{2\pi\varrho}{\lambda_0}\sqrt{n_1^2 - n_2^2} < 2.401. \tag{2.62}$$

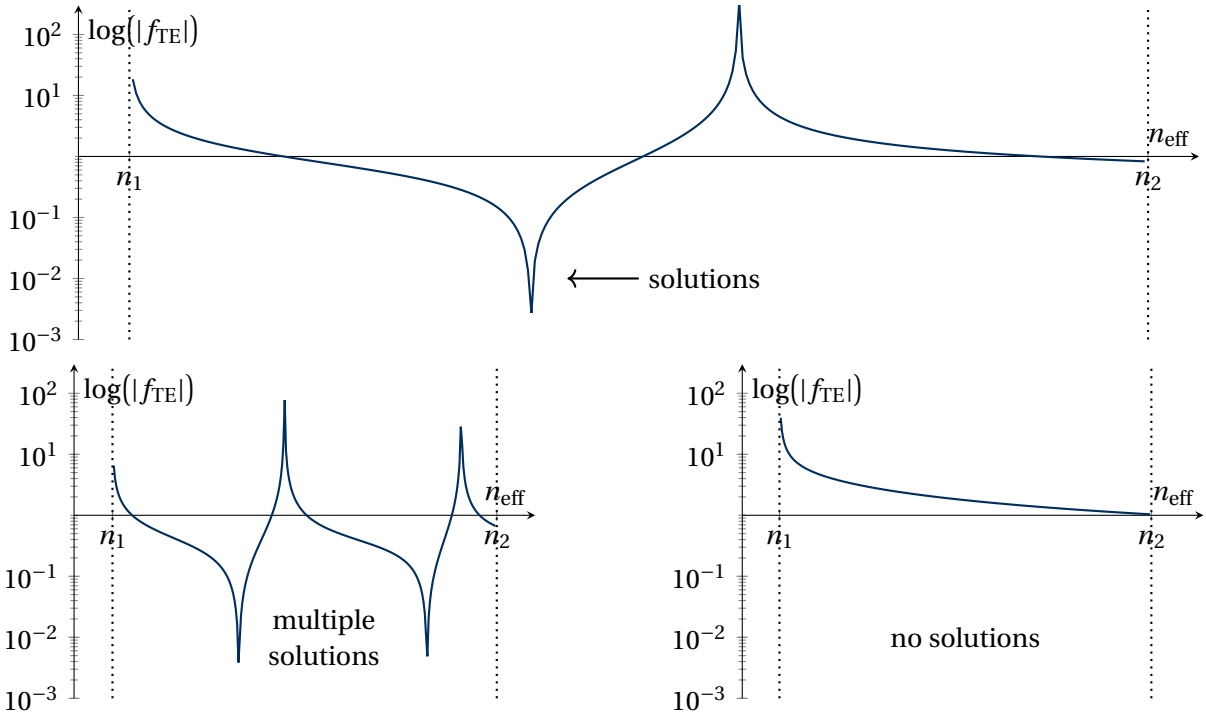

Figure 10: Top: Logarithmic plot of $|f_{TE}|$. The zeros of the function correspond to the solutions/modes of the fiber.
Bottom Left: In the case of a large ratio ϱ/λ_0 we find multiple zero crossings. Thus we have a multimode waveguide.
Bottom right: For a small ratio ϱ/λ_0 we do not find any solution.

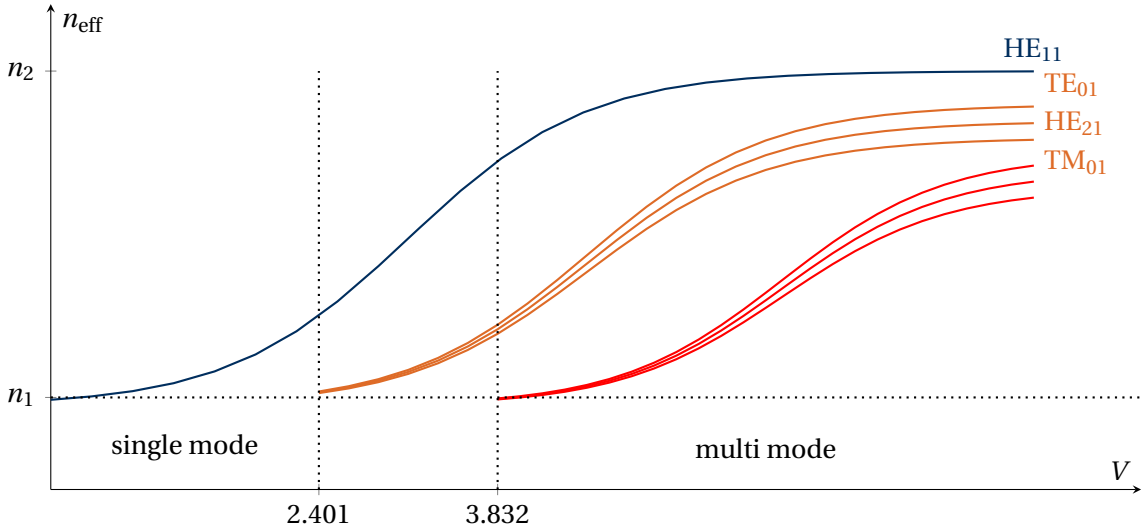

Figure 11: Dispersion plot of guided modes in fibers.

The number of modes M are hard to count (due to dispersion). We can find a rough approximation for large values of V as

$$M = \frac{4V^2}{\pi^2} + 2 \propto V^2. \tag{2.63}$$

For $V = 0$ we find $M = 2$ which corresponds to the degeneration of the fundamental HE_{11} mode.

Step 4: Calculate Modes

We start with the HE_{11}-mode. As shown in figure 12 it has a Gaussian type shape and most of the light is in the core. In the case of a small refractive index contrast the HE_{11}-mode is approximately linearly polarized.

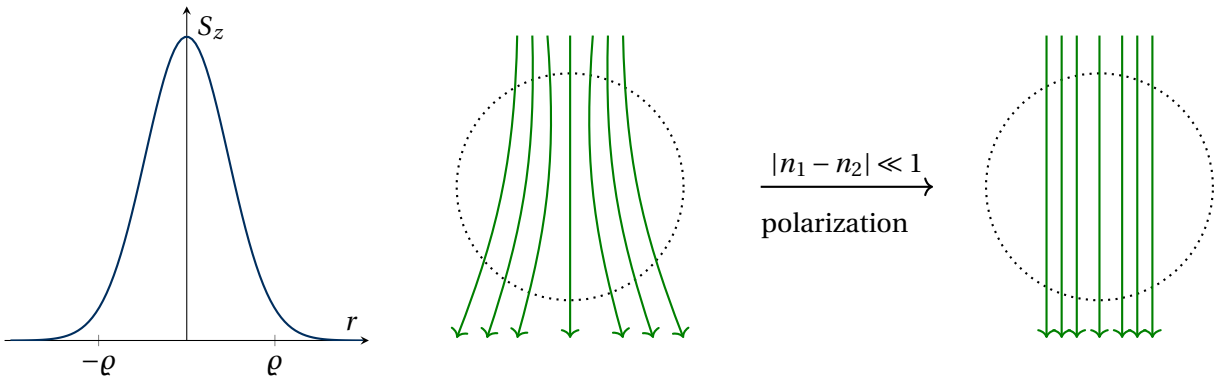

Figure 12: Transverse profile of the HE_{11}-mode. The electric field lines (green) are shown for the normal case (left) and small index contrast (right). However, for telecommunication applications, this approximation is valid.

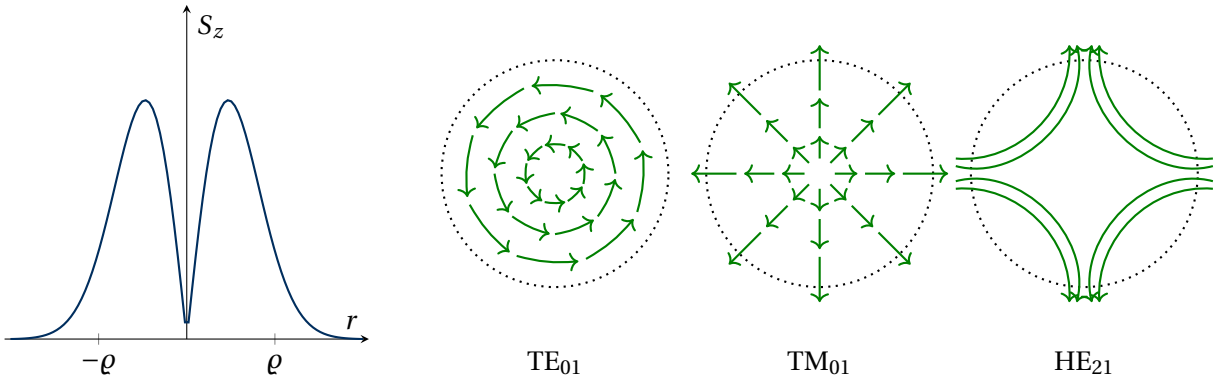

Figure 13: Transverse profile of the TE_{01}-, TM_{01}- and HE_{21}-mode. The electric field lines (green) are shown for all different polarizations. We observe that the TE_{01}-mode is azimuthally polarized, while the TM_{01}-mode is radially polarized.

2.1.4 Weakly guiding fibers

Many fibers have a small index contrast with $n_{\mathrm{cl}} \approx n_{\mathrm{co}}$. Then we may assume that all rays are paraxial and the transverse EM-field components dominate over the longitudinal components. For the weakly guided modes we assume the following approximations:

1. no longitudinal components: $E_z, H_z = 0$ (TEM-modes)
2. Transverse wave vector $\ll \beta$
3. The fields can be described in cartesian coordinates and fulfill the wave equation.

The transverse field then take the form

$$\boldsymbol{E}_l = F_l(R)\left[\cos(l\varphi)\hat{\mathbf{e}}_x - \sin(l\varphi)\hat{\mathbf{e}}_y\right]. \tag{2.64}$$

The wave equation is

$$\left[\frac{\partial^2}{\partial R^2} + \frac{1}{R}\frac{\partial}{\partial R} + \varepsilon k_0^2 - \beta^2 - \left(\frac{l}{R}\right)^2\right] F_l(R) = 0. \tag{2.65}$$

We can formulate the boundary conditions as

$$\text{BC1: } F_l^1(R=1) = F_l^2(R=1) \quad \text{and} \quad \text{BC2: } \left.\frac{\partial F_l^1}{\partial R}\right|_{R=1} = \left.\frac{\partial F_l^2}{\partial R}\right|_{R=1}. \tag{2.66}$$

Then we can make the following ansatz for the solutions $F_l(R)$

$$F_l(R) = A\begin{cases} \frac{J_l(UR)}{J_l(U)} & 0 \le R \le 1 (\text{core}) \\ \frac{K_l(WR)}{K_l(W)} & 1 < R < \infty (\text{cladding}). \end{cases} \tag{2.67}$$

This ansatz automatically fulfills boundary condition BC1. For boundary condition BC2 we find again by using $J_{l-1}(U) = -J_l'(U)$ and $K_{l-1}(W) = -K_l'(W)$ the dispersion equation of weakly guided fiber modes

Dispersion equation of weakly guided fiber modes

$$\frac{UJ_{l-1}(U)}{J_l(U)} = -\frac{WK_{l-1}(W)}{K_l(W)}. \tag{2.68}$$

The lowest order solution ($l = 0$) can be obtained by using $J_{-1} = J_1$ and $K_{-1} = K_1$

$$\underbrace{\frac{UJ_1(U)}{J_0(U)}}_{f^L} = \underbrace{+\frac{WK_1(W)}{K_0(W)}}_{f^R}. \tag{2.69}$$

Again we plot both functions and search for crossings (figure 14)

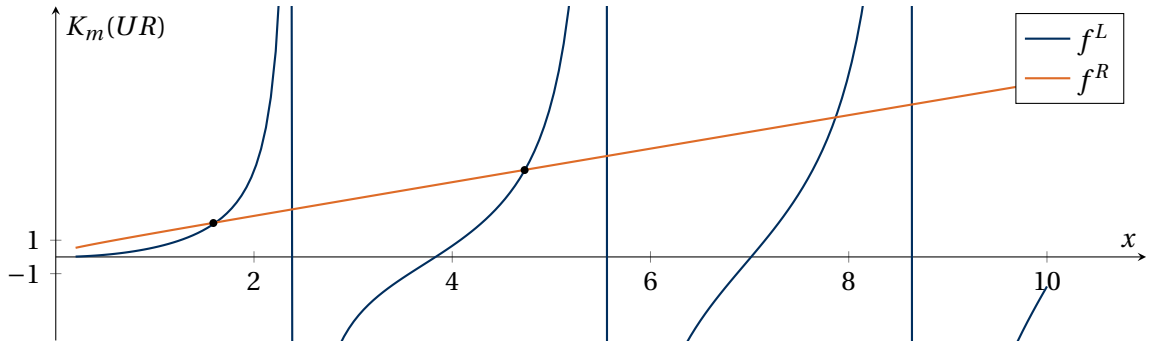

Figure 14: Graphical solution of equation (2.69). The nomenclature of the LP_{ln} modes is as follows: l describes the order of the Bessel function while n is the order of the root. The letters "LP" stand for *linearly polarized*.

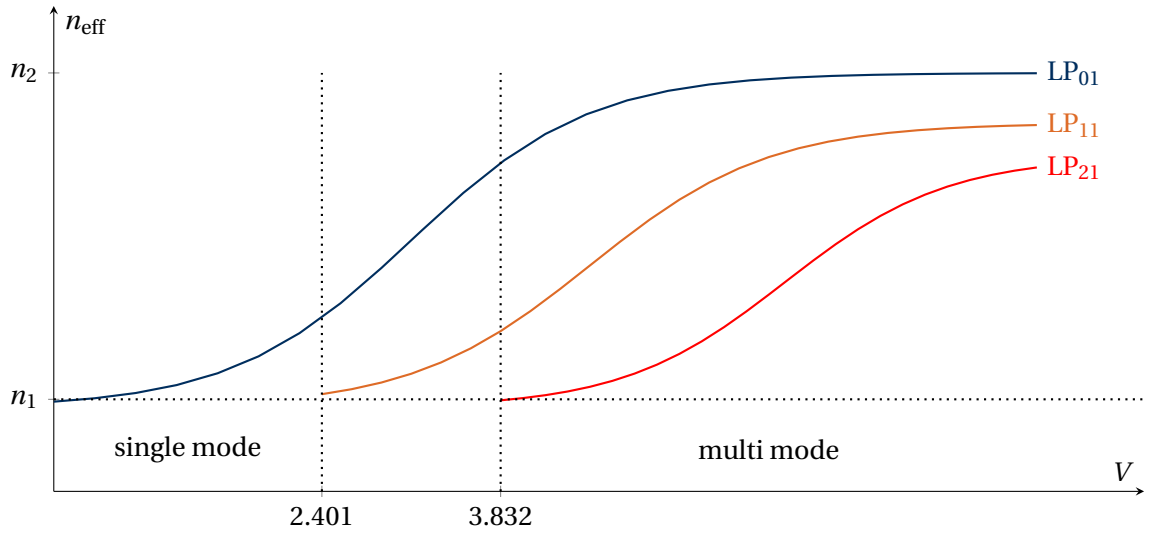

Figure 15: Dispersion plot of weakly guided modes in fibers. The weak guidance condition leads to a degeneration of higher-order modes.

2.2 Pulse propagation in fibers

The most relevant application of fibers is the support of optical pulses. This very important for telecommunication. Furthermore the nonlinear generation of light is also typically performed in fibers.

Pulse formation

The pulses are formed by a superposition of harmonics of different frequencies because Maxwells equations are linear. Let us discuss the example of *higher harmonics*

$$f(m,z,t) = \cos\big(\beta z - (\omega_0 + m\Delta\omega)\,t\big), \quad \text{with} \quad m \in \mathbb{Z}, \tag{2.70}$$

where ω_0 is the (central pulse) carrier frequency. $\Delta\omega$ is the spectral distance between the harmonics. The total pulse shape is now equal to

$$f_{\text{pulse}} = \sum_{m=-N}^{N} f_m(m,z,t), \tag{2.71}$$

where N is the number of the highest harmonic. Let us perform the summation at $z = 0$. Then we have

$$f_{\text{pulse}}(z=0) = \underbrace{\cos(\omega_0 t)}_{\text{carrier freq. oscil.}} \underbrace{\frac{\sin\big(\frac{\Delta\omega t}{2}(2N+1)\big)}{\sin\big(\frac{\Delta\omega t}{2}\big)}}_{\text{pulse envelope}} \tag{2.72}$$

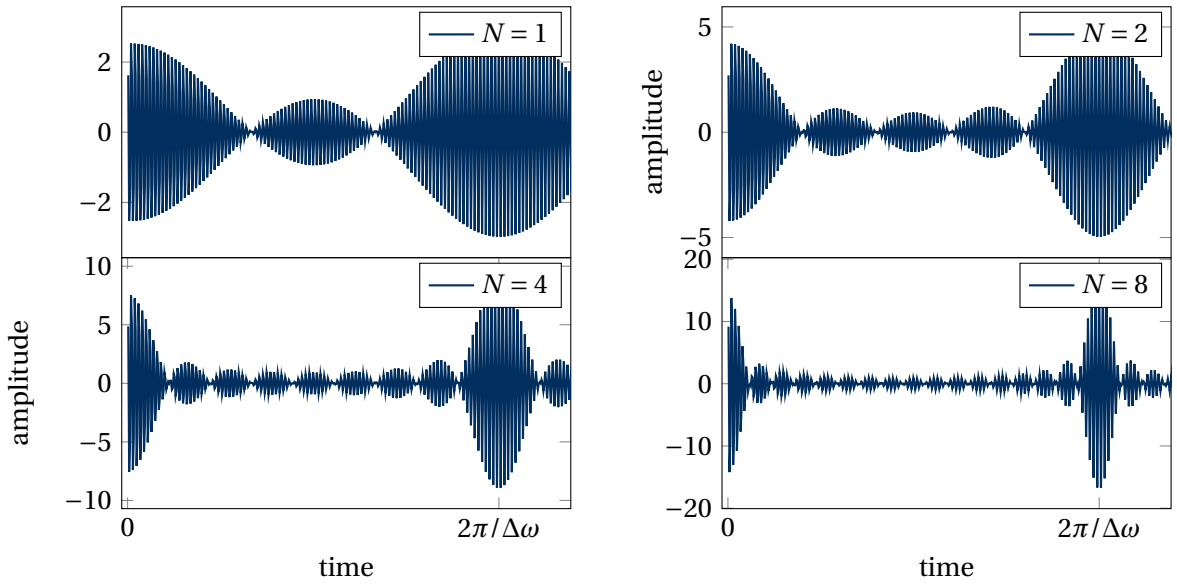

Figure 16: Visualization of the pulse field amplitude given by equation (2.72) for different values of N. Note that for higher orders N the maximum amplitude of the pulse increases. The distance between the maxima is called pulse separation time T_P.

Let us look at the pulse separation time T_P which can be calculated by looking at the zeros of the denominator term of (2.72)

$$0 = \sin\left(\frac{\Delta\omega T_P}{2}\right) \quad \Rightarrow \quad m\pi = \frac{\Delta\omega T_P^m}{2} \quad \Rightarrow \quad T_p = m\frac{2\pi}{\Delta\omega}. \tag{2.73}$$

Another quantity is the pulse carrier oscillation time $T_0 = \frac{2\pi}{\omega_0}$.

Let us make some statements summarizing our findings:

- The superposition of harmonics leads to the creation of pulse trains.
- The pulses are separated by T_P.
- The pulse train oscillates by the carrier frequency ω_0.
- An increasing number of harmonics leads to narrower pulses and increasing intensity.

Generally a pulse consists of the following parts:

1. Carrier phase $e^{-i\omega_0 t}$
2. Envelope function $A(z,t)$
3. Mode profile $U_0(x,y)$.

Therefore the total electric field at given point in space and time is

$$U(x,y,z,t) = U_0(x,y) \cdot A(z,t)e^{-i\omega_0 t} = U_0(x,y)F(z,t). \tag{2.74}$$

Pulse propagation in fibers

It is important to note that the different frequency components travel with different speed inside the fiber due to dispersion. This problem is illustrated in figure 17

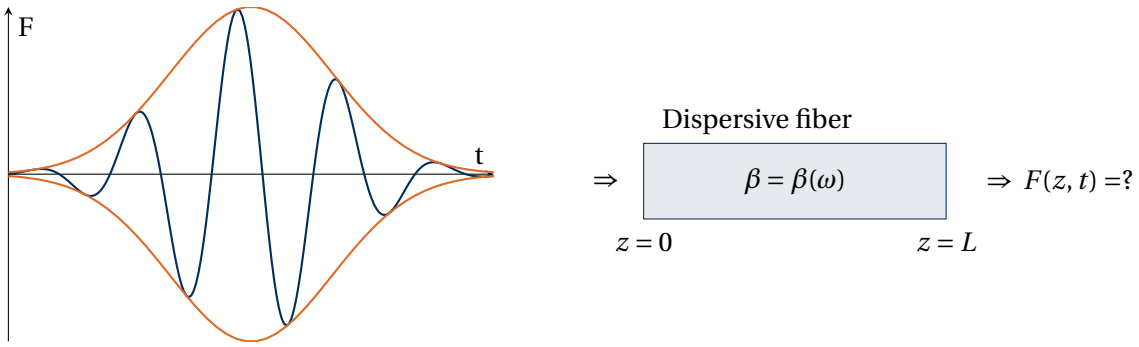

Figure 17: The pulse shape may change while propagation inside the fiber due to dispersion.

We can investigate this via a Fourier analysis of the propagation function

$$F(z,t) = \frac{1}{\sqrt{2\pi}} \int_{-\infty}^{\infty} \tilde{F}(z,\omega)e^{-i\omega t}\,d\omega\,. \tag{2.75}$$

Now we look at the spatial evolution of the component with the frequency ω

$$\tilde{F}(z,\omega) = \underbrace{A(z=0,\omega)\mathrm{e}^{-\mathrm{i}\omega_0 t}}_{\tilde{F}(z=0,\omega)}\mathrm{e}^{\mathrm{i}\beta(\omega)z}. \tag{2.76}$$

The term $\mathrm{e}^{\mathrm{i}\beta(\omega)z}$ describes the influence of the dispersion. It is also called *transfer function* because it transfers the frequency component to the localization z. $A(z=0,\omega)$ is the spectral distribution of the pulse envelope at the fiber input. Performing the evolution for each frequency components allows to retrieve the temporal shape of the pulse at location z

$$F(z,t) = \frac{1}{\sqrt{2\pi}}\mathrm{e}^{-\mathrm{i}\omega_0 t}\int A(z=0,\omega)\mathrm{e}^{i(\beta(\omega)z-\omega t)}\,\mathrm{d}\omega\,. \tag{2.77}$$

We want to emphasize that the dispersion $\beta(\omega)$ influences the output amplitude. The dispersion is in general a very complicated function, which implies that the integral cannot be solved analytically. A solution can be obtained via a Taylor expansion of $\beta(\omega)$ around the carrier frequency $\omega = \omega_0$

$$\beta(\omega) = \beta(\omega_0) + \beta'\Big|_{\omega_0}(\omega-\omega_0) + \frac{1}{2}\beta''\Big|_{\omega_0}(\omega-\omega_0)^2 + \ldots. \tag{2.78}$$

The first term is simply the inverse of the group velocity

$$\beta'\Big|_{\omega_0} = \frac{\mathrm{d}\beta}{\mathrm{d}\omega}\Big|_{\omega_0} = \frac{1}{v_g}\Big|_{\omega} = \beta_1. \tag{2.79}$$

We want to define a quantity called *group delay* τ_g

$$\tau_g = \frac{L}{v_g} \quad \text{with } L \text{ - fiber length.} \tag{2.80}$$

The second term is a measure of the dispersion of the speed of the frequency components and is therefore called *group velocity dispersion* (GVD)

$$\beta_2 = \beta''\Big|_{\omega_0} = \frac{\mathrm{d}^2\beta}{\mathrm{d}\omega^2}\Big|_{\omega_0}. \tag{2.81}$$

A nonzero GVD leads to temporal (not spectral) pulse broadening. Dispersion management is really important for telecommunication since if two pulses overlap due to large broadening, they cannot be distinguished anymore.

Let us define the *dispersion parameter* D

$$D = -\frac{\omega_0^2}{2\pi c_0}\beta_2. \tag{2.82}$$

Then we can write the dispersion function as

$$\beta(\omega) = \beta(\omega_0) + \frac{\omega-\omega_0}{v_g} - \underbrace{\frac{\pi c_0}{\omega_0}D(\omega-\omega_0)^2}_{\text{pulse dispersion}}. \tag{2.83}$$

Let us go back to the Fourier analysis and look what happens if we include the approximation of the transfer function

$$\begin{aligned}\tilde{F}(z=0,\omega) &= \frac{1}{\sqrt{2\pi}}\int_{-\infty}^{\infty} A(t')\mathrm{e}^{\mathrm{i}(\omega-\omega_0)t'}\,\mathrm{d}t' \\ \tilde{F}(z,t) &= \frac{1}{2\pi}\mathrm{e}^{\mathrm{i}(\beta(\omega_0)z-\omega_0 t)}\int_{-\infty}^{\infty}\left[\int_{-\infty}^{\infty} A(t')\mathrm{e}^{\mathrm{i}(\omega-\omega_0)t'}\,\mathrm{d}t'\right]\mathrm{e}^{\mathrm{i}\left(\frac{\omega-\omega_0}{v_g}z-\frac{\pi c_0}{\omega_0}D(\omega-\omega_0)^2 z-\omega t\right)}\,\mathrm{d}\omega \\ &= \frac{1}{2\pi}\mathrm{e}^{\mathrm{i}(\beta(\omega_0)z-\omega_0 t)}\int_{-\infty}^{\infty}\left[\int_{-\infty}^{\infty} A(t')\mathrm{e}^{\mathrm{i}(\omega-\omega_0)t'}\,\mathrm{d}t'\right]\mathrm{e}^{\mathrm{i}\left(\beta'(\omega-\omega_0)z+\frac{1}{2}\beta''(\omega-\omega_0)^2 z-\omega t\right)}\,\mathrm{d}\omega\,.\end{aligned} \tag{2.84}$$

We want to calculate the shape of the pulse explicitly for the example of a Gaussian shaped input pulse

$$F(t) = \mathrm{e}^{-(\frac{t}{\tau_p})^2}\mathrm{e}^{-\mathrm{i}\omega_0 t}. \tag{2.85}$$

Let us start with *case 1* of $D = 0 = \beta''$. The resulting envelope is

$$F(z,t) = \exp\left(\frac{(t-z\beta_1)^2}{\tau_p^2}\right)\mathrm{e}^{\mathrm{i}(\beta(\omega_0)z-\omega_0 t)}. \tag{2.86}$$

We observe that the pulse shape is conserved, as all frequency components travel with the same speed. We can see that the maximum of the pulse is located at

$$t = L(z)\beta_1 = \frac{L(z)}{v_g}. \tag{2.87}$$

We can now define the time of the moving frame $T = t - \frac{L}{v_g}$. Then we have

$$F(z=L,t) = \exp\left(\frac{T^2}{\tau_p^2}\right)\mathrm{e}^{\mathrm{i}(\beta(\omega_0)z-\omega_0 t)}. \tag{2.88}$$

Thus the pulse has the same shape for all values of L.

Let us move on to *case 2* with $\beta'' \neq 0$. The final result is

$$\begin{aligned}F(z,t) &= \frac{1}{\sqrt{1+\mathrm{i}\frac{2\beta_2 z}{\tau_p^2}}}\exp\left(-\frac{(t-z\beta_1)^2}{\mathrm{i}2z\beta_2+\tau_p^2}\right)\mathrm{e}^{\mathrm{i}(\beta(\omega_0)z-\omega_0 t)} \\ &= \underbrace{\frac{1}{\sqrt{1+\mathrm{i}\frac{2\beta_2 z}{\tau_p^2}}}}_{\text{amplitude change}}\underbrace{\exp\left(-\frac{(t-z\beta_1)^2\tau_p^2}{4z^2\beta_2^2+\tau_p^4}\right)}_{\text{width change}}\underbrace{\exp\left(\mathrm{i}\frac{2z\beta_2(t-z\beta_1)}{4z^2\beta_2^2+\tau_p^4}\right)}_{\text{local phase influence}}\underbrace{\mathrm{e}^{\mathrm{i}(\beta(\omega_0)z-\omega_0 t)}}_{\text{carrier phase}}.\end{aligned} \tag{2.89}$$

For an nonzero GVD the temporal pulse width increases.

Pulse width analysis

We now want to consider how the GVD influences the pulse width. For that we define the *pulse width level B* as shown in figure 18. For our discussion we use $B = e^{-1/4}$. Then the pulse width at z is given by

$$\begin{aligned}\tau(z) &= \tau_p \sqrt{1 + \left(\frac{2z\beta_2}{\tau_p}\right)^2} \\ &= \tau_p \sqrt{1 + \left(\frac{4c_0 D\pi z}{\tau_p^2 \omega_0^2}\right)^2}.\end{aligned} \tag{2.90}$$

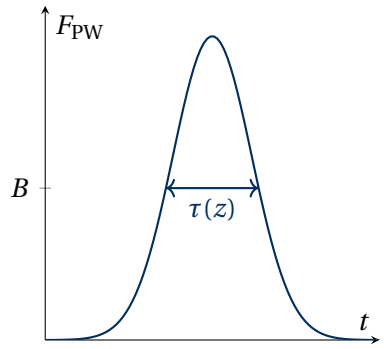

Figure 18: Pulse width term of (2.89).

In the following we want to plot the puls length for different β_2 values and different starting pulse lengths τ_p.

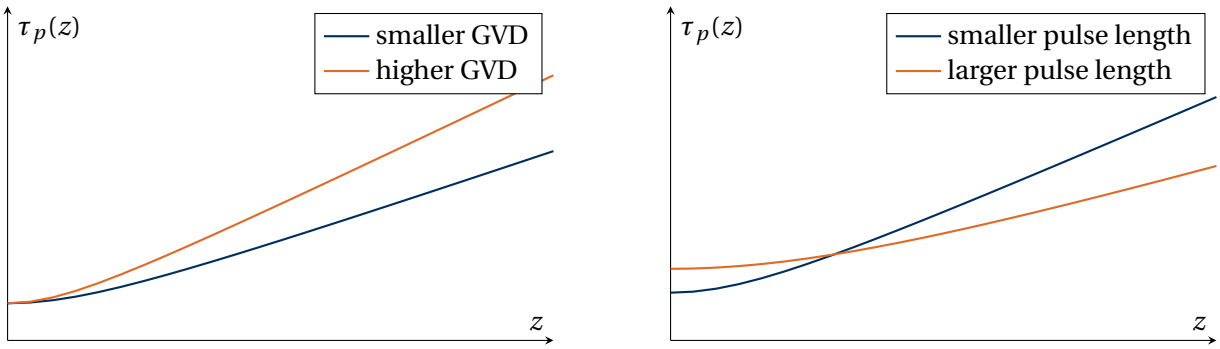

Figure 19: Left: We observe that larger GVD leads to a faster pulse dispersion.
Right: Short pulses disperse at a faster rate.

We now define the *Pulse width doubling distance* given by

$$2\tau_p = \tau_p \sqrt{1 + \left(\frac{2z_D\beta_2}{\tau_p}\right)^2} \quad \Rightarrow \quad z_D = \left|\frac{\sqrt{3}\tau_p^2}{2\beta_2}\right|. \tag{2.91}$$

Let us discuss the example of fused silica at $\lambda_0 = 1{,}55\,\mu\mathrm{m}$. Here we have

$$D = 21\,\frac{\mathrm{ns}}{\mathrm{km\,mm}} \quad \text{or} \quad \beta_2 = -26{,}8\,\frac{\mathrm{fs}^2}{\mathrm{mm}}. \tag{2.92}$$

Then we can easily calculate the pulse doubling distances for different pulse lengths

$$z_D(1\,\mathrm{fs}) = 32{,}3\,\mu\mathrm{m}, \quad z_D(1\,\mathrm{ps}) = 32{,}3\,\mathrm{m}, \quad z_D(1\,\mathrm{ns}) = 32\,300\,\mathrm{km}. \tag{2.93}$$

Since femtosecond pulses disperse on micro meter ranges, they are not suitable for telecommunciation.

Local phase

Let us now consider the temporal distribution of the phase at position z

$$\Phi(z,t) = \underbrace{\frac{2z\beta_2(t-z\beta_1)^2}{4z^2\beta_2^2+\tau_p^4}}_{\text{local modification}} + \underbrace{\beta(\omega_0)z-\omega_0 t}_{\text{carrier phase}}. \tag{2.94}$$

The local frequency is given as the time derivative of the local phase at z

$$\omega_c(z,t) = \frac{\partial\Phi(z,t)}{\partial t} = \underbrace{\frac{2z\beta_2(t-z\beta_1)}{4z^2\beta_2^2+\tau_p^4}}_{\text{local modification}} - \omega_0 = \omega_m(z,t) - \omega_0. \tag{2.95}$$

In figure 20 we can see the effect of a nonzero GVD on the pulse shape. In the first case of $\beta_2 = 0 \Rightarrow \omega_m = 0$ we do not observe a chirp. In the second case $\beta_2 > 0 \Rightarrow \omega_m \neq 0$ a chirp of frequency along the pulse is visible.

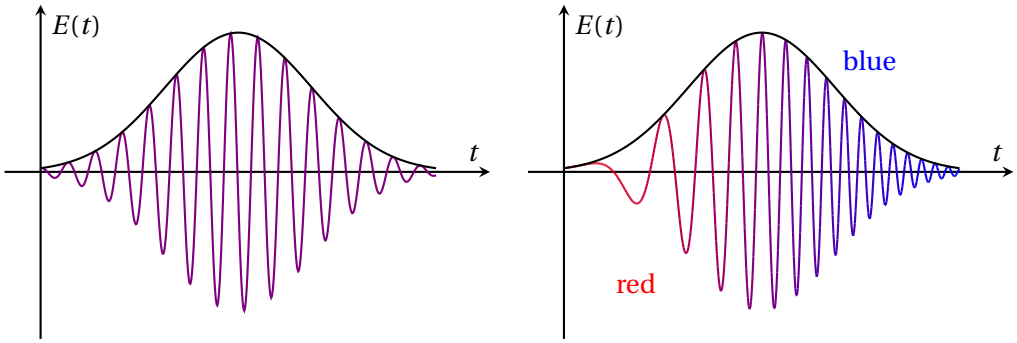

Figure 20: Depiction of the amplitude of the electric field $F(z,t)$ and its envelope (black) according to (2.89) without a chirped temporal phase $\varphi(t) = \beta(\omega_0)z - \omega_0 t$ (left) and with a linearly chirped temporal phase $\varphi(t) = A(t-z\beta_1)^2 + \beta(\omega_0)z - \omega_0 t$ (right).

We can distinguish two different kinds of dispersion:

$$\begin{aligned} D<0, \beta_2>0 \quad & \text{normal dispersion} \\ D>0, \beta_2<0 \quad & \text{anomalous dispersion.} \end{aligned} \tag{2.96}$$

We conclude that the dispersion is key for pulse propagation in fibers.

Types of dispersion

The first type of dispersion we want to discuss is *material dispersion* $n = n(\omega)$. We will consider the following on the example of fused silica glass.

We can define the so called dispersion wavelength λ_{ZDW} at which the group velocity dispersion is zero. Here the behavior of the medium changes from normal dispersion to anomalous dispersion.

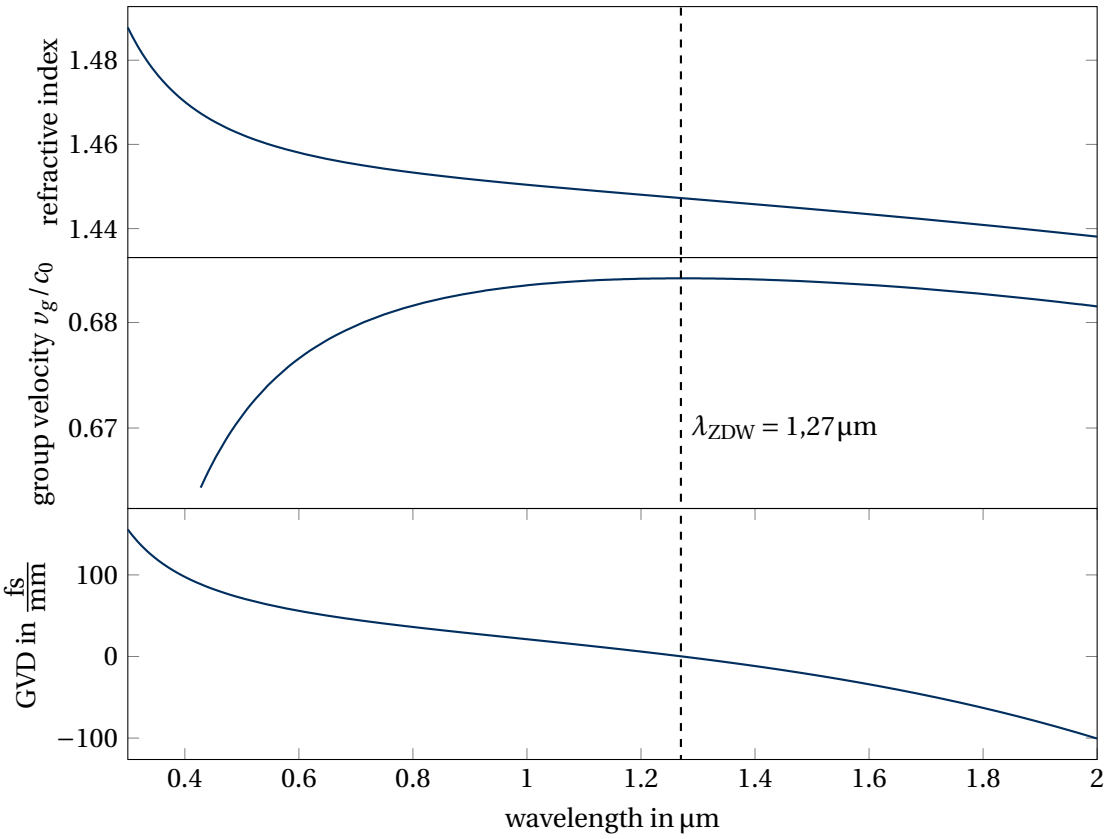

Figure 21: Refractive index of fused silica in a wavelength range of 0,3 µm...2 µm obtained from https://refractiveindex.info/?shelf=glass&book=fused_silica. The group velocity and group velocity dispersion were calculated from the refractive index.

The second type is *waveguide dispersion* $\beta = \beta(\omega_0)$. It results from the spectral dependence of the overlap of the mode with the core and cladding.

The third type is *intermodal dispersion*. Here, different modes have different distributions of $\beta = \beta(\omega)$. The origin is a different fraction of power in the core and cladding. This is relevant between fundamental (HE_{11}, TE_{01}) and higher order modes.

This especially important for fibers with two degenerate fundamental modes. By deforming the core, the degeneration of the fundamental modes is removed. The result is a change of polarization state along the fiber. Therefore the fiber exhibits a waveplate like behaviour.

Therefore we define the *birefringence* B as

$$B = \frac{|\beta_x - \beta_y|}{k_0} = |n_{\mathrm{eff}}^x - n_{\mathrm{eff}}^y|. \tag{2.97}$$

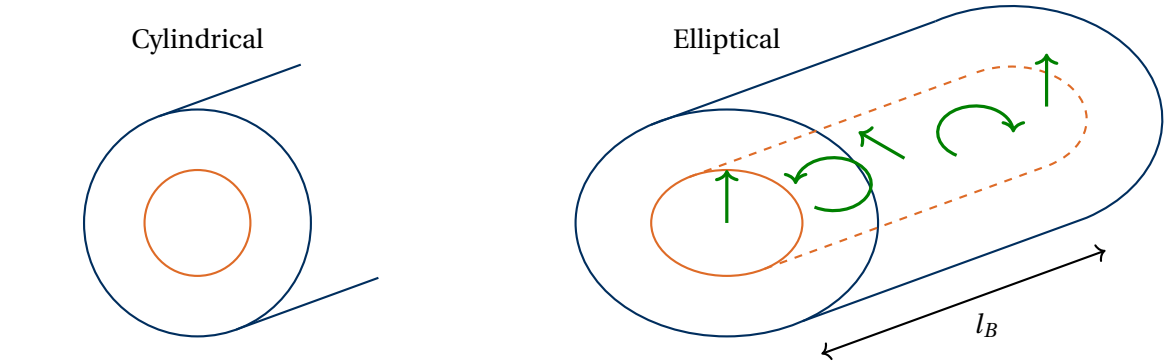

Two degenerated fundamental modes $\beta_x = \beta_y$

Fundamental modes are not degenerated $\beta_x \neq \beta_y$

Figure 22: For an elliptical fiber the degeneration of the two fundamental modes in x- and y-direction is lifted. This leads to a polarization mode dispersion. The distance, after which the inital polarization state is recovered is called *beat length*.

Using the evolution of the eigenstates $E_x \sim \mathrm{e}^{\mathrm{i}\beta_x z}$ and $E_y \sim \mathrm{e}^{\mathrm{i}\beta_y z}$ the change of polarization along the fiber is described by the polarization parameter

$$\chi = \frac{E_y}{E_x} = \mathrm{e}^{\mathrm{i}(\beta_x - \beta_y)z}. \tag{2.98}$$

The polarization parameter is recovered for $|\beta_x - \beta_y| l_B = 2\pi$. Thus we have

$$l_B = \frac{2\pi}{|\beta_x - \beta_y|} = \frac{\lambda_0}{B}. \tag{2.99}$$

An example is the polarization maintaining fiber (PMF). It is fabricated by placing two stress-rods on the core (gray circles). The stress rods put stress on the core thus changing the refractive index for the two different polarization directions. For a birefringence of $B \approx 10^{-4}$ and a wavelength of $\lambda = 1\,\mu\mathrm{m}$ the beat length is $l_B = 1\,\mathrm{cm}$.

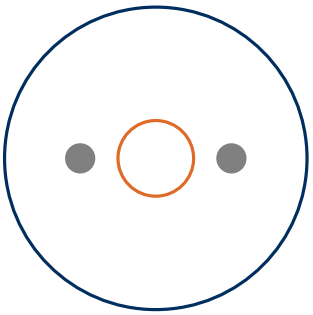

For an optical pulse propagation the two eigenstates appear at the fiber output at different times determined by the group velocity. Therefore we define the *group delay difference* as

$$\Delta\tau_{\mathrm{GD}} = \frac{L}{v_g^y} - \frac{L}{v_g^x} = L\left(\frac{\partial\beta_y}{\partial\omega}\bigg|_{\omega_0} - \frac{\partial\beta_x}{\partial\omega}\bigg|_{\omega_0}\right). \tag{2.100}$$

A typical value for a low birefringent fiber would be $\frac{\Delta\tau_{\mathrm{GD}}}{L} = 1\,\frac{\mathrm{ps}}{\mathrm{km}}$.

3 Materials and Fabrication

3.1 Attenuation in fibers

The power in fiber decreases exponentially along the propagation direction. We can define an *attenuation coefficient* α as

$$P = P_0 \exp(-\alpha z) \tag{3.1}$$

as in Lambert-Beers law. Mathematically, the attenuation leads to a complex propagation constant

$$\beta = \beta_R + \mathrm{i}\beta_I \quad \text{and} \quad n_{\text{eff}} = n_{\text{eff}}^R + \mathrm{i}n_{\text{eff}}^I. \tag{3.2}$$

The wave is then attenuated in the fiber like

$$E(x,y,z) = E_0 \mathrm{e}^{\mathrm{i}\beta_R z} \mathrm{e}^{-\beta_I z}. \tag{3.3}$$

Now using that $\frac{P}{P_0} = \frac{|E|^2}{|E_0|^2}$ we find the attenuation coefficient as

$$\alpha = 2\beta_I. \tag{3.4}$$

Most commonly the attenuation is given via a power loss coefficient

$$\gamma = \frac{10}{L} \log_{10} \frac{P}{P_0} \quad [\text{dB/m}]. \tag{3.5}$$

We can rewrite this by using $\frac{P}{P_0} = 10^{\frac{\gamma L}{10}} = \mathrm{e}^{-\alpha L}$ in terms of the attenuation coefficient

$$\gamma = -\frac{10}{\ln 10}\alpha \approx -4.343\alpha \quad \gamma\,[\text{dB/m}] = -4.343\,\alpha \left[\frac{1}{\text{m}}\right] \tag{3.6}$$

3.2 Fundamental of light-matter interaction

In the following we want to discuss the different origins of dispersion and attenuation which can be categorized into two groups, absorption and scattering.

absorption	scattering
electronic (UV)	elastic: Rayleigh
vibrational (MID-IR)	inelastic: Raman (optical)
impurities (NEAR-IR)	inelastic: Brillouin (acoustic)

3.2.1 Absorption

At first we want to briefly repeat the theory of material dispersion starting at the polarization $\boldsymbol{P}(t)$ which is generated by an electric field. In the following we a assume a linear response function connecting polarization and electric field. In the theory of response functions the polarization is given as a convolution of response function $R(\tau)$ and electric field

$$\begin{aligned}
\boldsymbol{P}(t) &= \varepsilon_0 \int_{-\infty}^{\infty} \mathrm{d}\tau\, R(\tau)\boldsymbol{E}(t-\tau) \\
\Rightarrow \boldsymbol{P}(\omega) &= \frac{\varepsilon_0}{\sqrt{2\pi}} \int_{-\infty}^{\infty} \mathrm{d}t \int_{-\infty}^{\infty} \mathrm{d}\tau\, R(\tau)\boldsymbol{E}(t-\tau)\mathrm{e}^{-\mathrm{i}\omega t} = \frac{\varepsilon_0}{\sqrt{2\pi}} \int_{-\infty}^{\infty} \mathrm{d}t' \int_{-\infty}^{\infty} \mathrm{d}\tau\, R(\tau)\boldsymbol{E}(t')\mathrm{e}^{-\mathrm{i}\omega(t'+\tau)} \\
&= \varepsilon_0 \underbrace{\frac{1}{\sqrt{2\pi}} \int_{-\infty}^{\infty} \mathrm{d}t'\, \boldsymbol{E}(t')\mathrm{e}^{-\mathrm{i}\omega t'}}_{\boldsymbol{E}(\omega)} \underbrace{\int_{-\infty}^{\infty} \mathrm{d}\tau\, R(\tau)\mathrm{e}^{-\mathrm{i}\omega\tau}}_{\chi^{(1)}(\omega)} = \varepsilon_0 \chi^{(1)}(\omega)\boldsymbol{E}(\omega).
\end{aligned} \tag{3.7}$$

Now using the definition of the displacement field $\boldsymbol{D} = \varepsilon_0\boldsymbol{E} + \boldsymbol{P}$ we can introduce the *dielectric function*

$$\boldsymbol{D} = \varepsilon_0(1+\chi^{(1)})\boldsymbol{E} = \varepsilon_0\varepsilon\boldsymbol{E}. \tag{3.8}$$

the dielectric function is a frequency dependent, complex quantity containing all material properties and microscopic interactions.

Now we would like to discuss the origin of the complex dielectric function. Essentially, the electric field displaces the electrons in the crystal lattice of the dielectric materials while the nuclei stay fixed. This creates a center of mass of negative charges displaced from the nucleus. With the distance $\boldsymbol{d}$ to the nucleus we can define a dipole moment $\boldsymbol{p} = q\boldsymbol{d}$. The response of the dipoles can be characterized via a *polarizability* α_p given as

$$\boldsymbol{p} = \alpha_p\boldsymbol{E} = q\boldsymbol{d}. \tag{3.9}$$

The macroscopic polarization is then given by the sum of all dipole moments per unit of volume. This corresponds to a multiplication with the dipole density since all dipoles are pointing in the same direction

$$\boldsymbol{P} = N\boldsymbol{p} = N\alpha_p\boldsymbol{E}. \tag{3.10}$$

Comparing this to the expression for the polarization (3.7) we find

$$\varepsilon = 1 + \frac{N}{\varepsilon_0}\alpha_p. \tag{3.11}$$

We observe that the microscopic dipole response is connected to the macroscopic material property ε. Note, that equation (3.11) only holds for low density media, where interactions between dipoles can be neglected.

Lorentzian oscillator model

In the following we want to develop a mathematical expression for the polarizability α_p. Here, the electrons are assumed to be driven, damped harmonic oscillators satisfying the following equation

$$m\ddot{r} + m\gamma\dot{r} + m\omega_0^2 r = -eE_0 e^{-i\omega t}. \tag{3.12}$$

Now using $\boldsymbol{r} = \frac{\alpha_p}{q}\boldsymbol{E}$ we solve this for the polarizability and arrive at

$$\alpha_p = \frac{e^2}{m}\frac{1}{(\omega_0^2 - \omega^2) - i\gamma\omega} = A_\alpha e^{i\varphi_\alpha}. \tag{3.13}$$

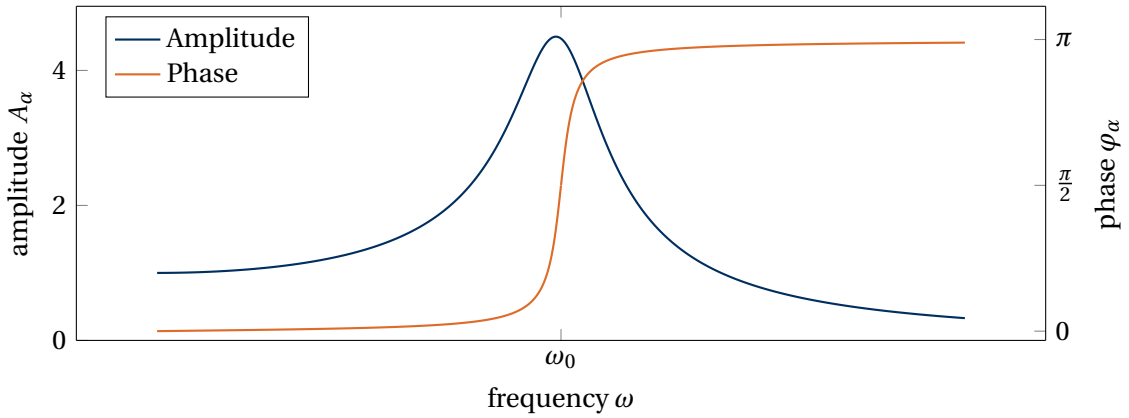

Figure 23: Amplitude and phase of the complex polarizability α_p.

Then we can write down the dielectric function

$$\varepsilon = 1 + \frac{N}{\varepsilon_0}\alpha_p = 1 + \frac{\omega_p^2}{\omega_0^2 - \omega^2 - i\gamma\omega} \quad \text{with} \quad \omega_p^2 = \frac{Ne^2}{\varepsilon_0 m} \tag{3.14}$$

and also plot its real part as shown in figure 24.

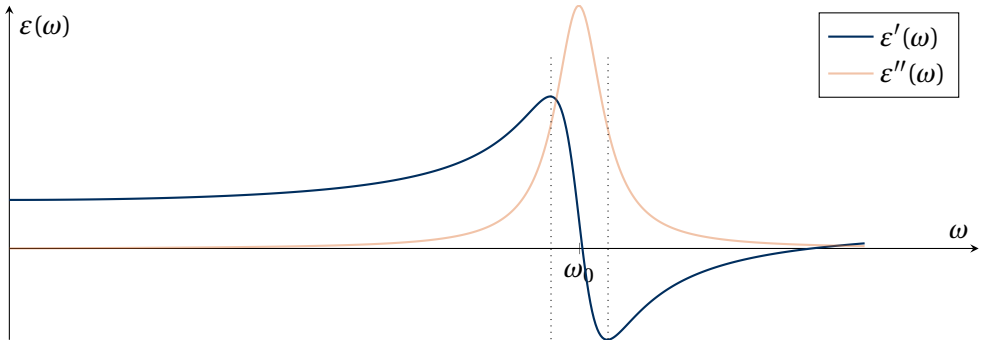

Figure 24: Real- and imaginary part of the dielectric constant. In the area bounded by dashed lines we have anomalous dispersion $\frac{d\varepsilon}{d\omega} < 0$ whereas outside we have normal dispersion $\frac{d\varepsilon}{d\omega} > 0$. In a frequency range above the resonance is a small area, where the dielectric constant is negative. This corresponds to the case of a metal.

If the material has multiple resonances we can describe it as a collection of different oscillators

$$\varepsilon = 1 + \omega_p^2 \sum_j \frac{f_j}{(\omega_{0,j}^2 - \omega^2) - \mathrm{i}\gamma_j \omega} \quad f_j \text{ - oscillator strength.} \tag{3.15}$$

The general response of a nonconducting material consists of several parts in different wavelength regimes. In the microwave range we find oscillations of ions (Debye relaxations). In the infrared part resonances are cause by molecule vibrations, whereas in the visual spectrum electric resonances play an important role.

Sellmeier model

We now want to apply the Lorentz oscillation model to real dielectric materials. In wavelength ranges where materials are transparent we will be far away from a resonance and therefore absorption can be neglected $\gamma \approx 0$. Then we can find the following formula for the refractive index which is called *Sellmeier formula*

$$n^2 = 1 - \sum_j \frac{A_j \lambda_j}{\lambda_{0,j}^2 - \lambda_j}. \tag{3.16}$$

For fused silica the refractive index profile was shown already in figure 21. Here the valid wavelength range of the Sellmeier formula is 0,3 µm…2 µm.

In order to approximate absorption a commonly used model is called *Urbach Tail* model. Here we also assume a range far away from a resonance. Here the absorption α can be approximated as

$$\alpha(E) = \alpha_0 \mathrm{e}^{\frac{E}{E_U}} \quad \text{with } E_U \text{ Urbach energy.} \tag{3.17}$$

3.2.2 Scattering processes

Scattering processes can induce frequency shifts, where the new central frequency lies at

$$\nu_{\text{new}} = \nu_0 \pm \nu_S, \tag{3.18}$$

where in the case $-\nu_S$ (smaller energy) we speak of a Stokes line whereas $+\nu_S$ is called Anti-Stokes line.

Table 2: Different types of scattering in a material

origin	Type of scattering	ν_S
Inhomogeneities	Rayleigh scattering	0
Molecular vibrations	Raman scattering	0,3 THz…30 THz
Acoustic phonons	Brillouin scattering	≈ 3 GHz

Rayleigh scattering

In a classical picture Rayleigh scattering in a fiber results from index fluctuations which are randomly disctributed inside the fiber. However, for our model we need to make some assumptions:

- Small fluctuations: $\overline{(\varepsilon - \bar{\varepsilon})^2} \ll \bar{\varepsilon}^2$
- Fast spatial fluctuations: $l_{\text{correlation}} \ll \lambda$.

We now assume an ensemble of dipoles where each dipole is a source of energy loss. Then the average power losss is given by

$$\langle P_D \rangle = \frac{\mu_0 |\pm p|^2 \omega^4}{12\pi c_0} \sim \frac{1}{\lambda^4}. \tag{3.19}$$

A statistical treatment yields

$$P(z) = P_0 \mathrm{e}^{-\alpha_{\text{RLS}} z} \quad \text{with} \quad \alpha_{\text{RLS}} = \frac{8\pi^3}{3\lambda_0^4} V_s, \tag{3.20}$$

where V_s is called the scattering volume. V_s is of the order of $10^{-31}\,\mathrm{m}^3 \ldots 10^{-30}\,\mathrm{m}^3$ and is a material constant.

Raman scattering

For the description of Raman scattering we follow the classical approach of an oscillating diatomic molecule like C-H which can be described as two masses coupled by a spring. Then Hooke's law states

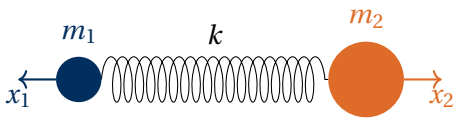

$$\underbrace{\frac{m_1 m_2}{m_1 + m_2}}_{\mu} (\ddot{x}_1 + \ddot{x}_2) = -k \underbrace{(x_1 + x_2)}_{q}. \tag{3.21}$$

Using the reduced mass μ and a normal coordinate q, the differential equation is simplified to

$$\mu \ddot{q} = -kq \quad \Rightarrow \quad q = q_0 \cos(\omega_R t) \quad \text{with} \quad \omega_R^2 = \frac{k}{\mu}. \tag{3.22}$$

Note that each molecular unit has its own resonance frequency. Since molecular vibrations change the polarizability, α_p will be expanded into a Taylor series around the equilibrium state (average polarizability α_p^0)

$$\alpha_p(q) = \alpha_p^0 + \left(\frac{\partial \alpha_p}{\partial q}\right)_{q=0} q + \ldots \approx \alpha_p^0 + \alpha_p' q, \tag{3.23}$$

where α'_p describes the deviation of α_p from the equilibrium state. For a light wave of the form $E(t) = E_0 \cos(\omega_0 t)$ the dipole moment can be computed as

$$\begin{aligned} p(t) = \alpha_p(t)E(t) &= \alpha_p^0 E_0 \cos(\omega_0 t) + \alpha'_p q_0 \cos(\omega_R t)\cos(\omega_0 t) \\ &= \underbrace{\alpha_p^0 E_0 \cos(\omega_0 t)}_{\text{RLS}} + \underbrace{\frac{\alpha'_p}{2} q_0 \Big[\underbrace{\cos((\omega_0+\omega_R)t)}_{\text{Anti Stokes RLS}} + \underbrace{\cos((\omega_0-\omega_R)t)}_{\text{Stokes RLS}} \Big]}_{\text{Inelastic scattering}} \end{aligned} \tag{3.24}$$

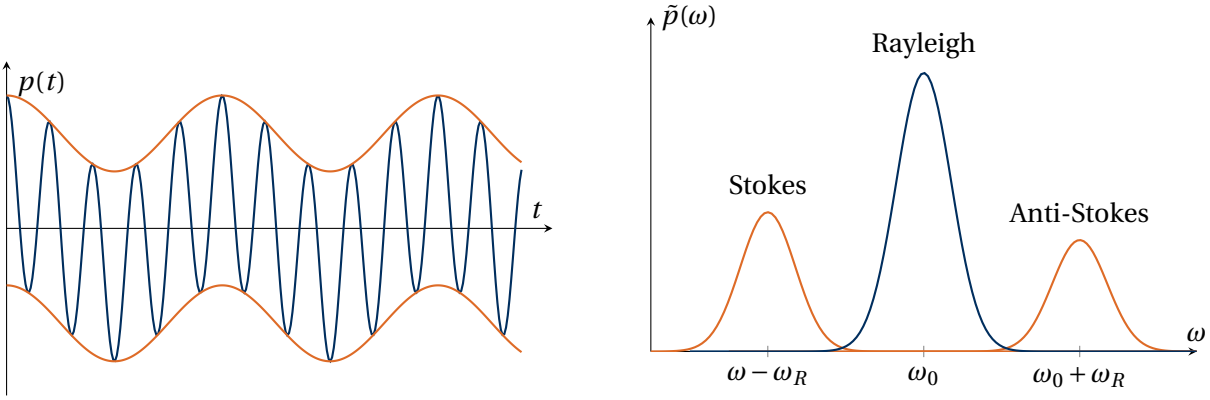

Figure 25: Left: Plot of the time dependent polarization $p(t)$. In blue we see the oscillations at the fundamental frequency ω_0 with a envelope given by the beating frequencies.
Right: Polarization in the frequency domain. Note that the Anti-Stokes Peak is lower than the Stokes-Peak. This effect cannot be explained classical, for that one has to use a quantum mechanical description.

3.3 Optical properties of silica glass

Nearly all produced optical fibers are based of silica glass (SiO_2). The main reasons for its success are:

- It is very transparent in the NIR.
- It is cheap to produce.
- It can be considered an ideal glass.

The building blocks of silica glass are silicon and oxygen. The silicon form [SiO_4] tetrahedrons where Si is in a sp^3-hybridization. The neighbouring tetrahedrons share oxygen Ions O^- with each other which leads to a network formation. However, there is no periodic order of the network formation. Therefore we observe only short-range order whereas in the long-range the material appears to be amorph. This is essentially the definition of a glass.

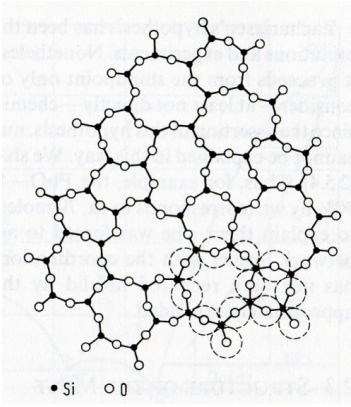

Figure 26: Silica network.

In the following we want to discuss loss mechanisms in fused silica. A loss spectrum is displayed in figure 27. Here we observe that the lowest attenuation occurs at 1,55 µm with a loss of $\gamma = 0{,}16\,\mathrm{dB/km}$.

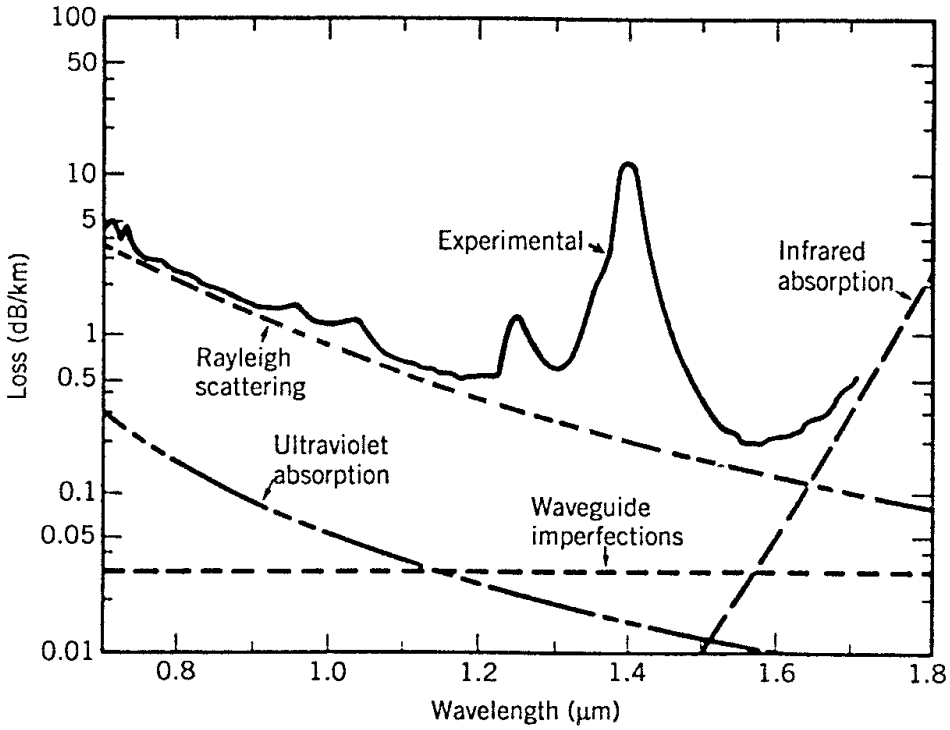

Figure 27: Loss spectrum of a single-mode fiber produced in 1979. Wavelength dependence of several fundamental loss mechanisms is also shown. From: Agrawal, Govind P. Fiber-optic communication systems. John Wiley & Sons, 2002

We now want to list the different channels of absorption in fused silica:

1. UV-absorption: The random environment of Si-O molecules leads to the formation of electronic bands with a bandgap of ≈ 106 nm. When being exposed to short wavelengths this can break the molecul bonds and slowly deterioate the material. The silica gets dark. This effect is called *solarization*.
2. VIS-attenuation: In the visible regime the absorption is dominated by Rayleigh scattering ($\sim 1/\lambda^4$).
3. Near-IR absorption: Since the fabrication of fused silica is never perfect, water can easily dissolve. This leads to the formation of hydroxic groups like $\equiv \mathrm{Si-O-Si} \equiv + \mathrm{H_2O} \longrightarrow \equiv \mathrm{Si-OH}$. The OH group gives large Absorption

Name	λ [µm]	Origin
ν_3	2.68	Fundamental anti-symmetric stretching mode
$\nu_3 + \nu_1$	2.20	Combination of fundamental OH mode + Tetrahedron mode
$2\nu_3$	1.37	First overtone of ν_3

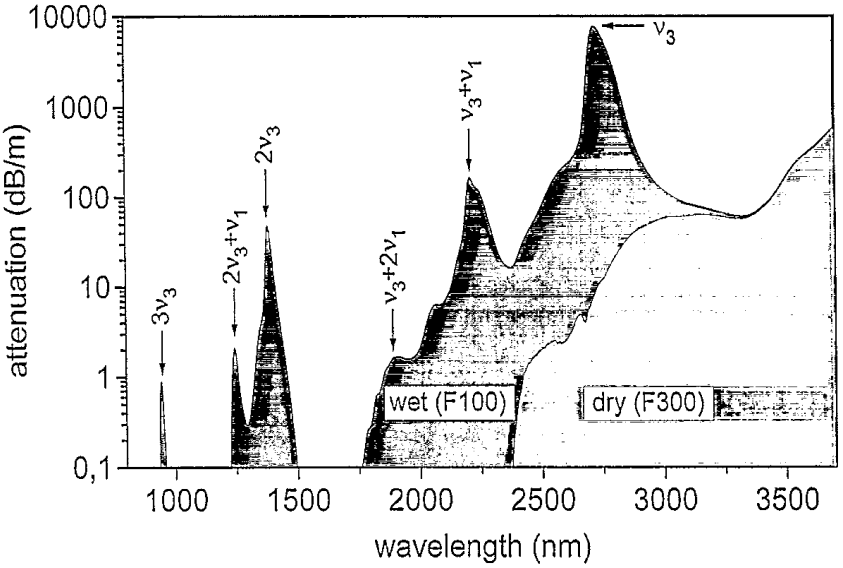

Figure 28: Light absorption of silica in the near infrared regime for dry and wet silica. Note that for wet silica the formation of hydroxic groups increases the absorption.

4. Mid-IR attenuation: The vibrational eigenmodes of the tetrahedron leads to very strong absorption for wavelengths $\lambda > 5\mu m$. Due to symmetry, 4 modes are relevant as shown in figure 29.

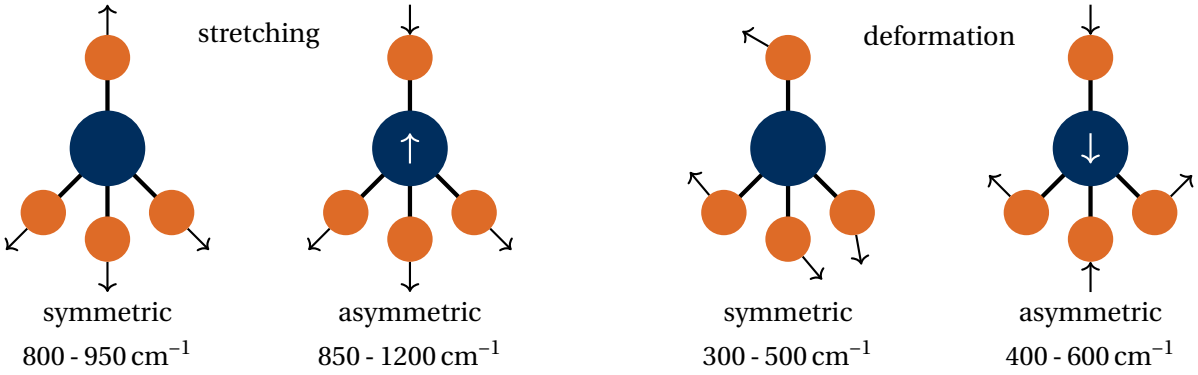

Figure 29: Vibrational eigenmodes of silica tetrahedron (blue: silicon, orange: oxygen).

In order to achieve two different refractive indices for core and cladding, one part is often doped to induce a refractive index change The most prominent examples are:

- Dopant: Germanium, refractive index increase
- Dopant: fluorine, refractive index decrease.

The index of the doped material is given via a mixed Sellmeier equation

$$n^2 = 1 - \sum_j \frac{(A_j^S + X(A_j^G - A_j^S))\lambda^2}{(\lambda_j^S + X(\lambda_j^G - \lambda_j^S)) - \lambda^2}, \quad X \text{ - fraction of } GeO_2. \tag{3.25}$$

Here A_j^S and A_j^G are the amplitudes of SiO_2 and GeO_2 and λ_j^S, λ_j^G their respective resonance wavelengths. If one increases the fraction of GeO_2 from zero to one, the refractive index changes approximately linear with increasing concentration from $n = 1.44$ to $n = 1.47$ ($X = 1$) for $\lambda = 1{,}3\,\mu m$.

3.4 Fiber implementation

First we want to note that the typical fabrication of fibers, *fiber drawing*, is not possible with crystalline materials with a well defined melting point. However, glass is a liquid at any temperature but rather changes in viscosity as seen in figure 30.

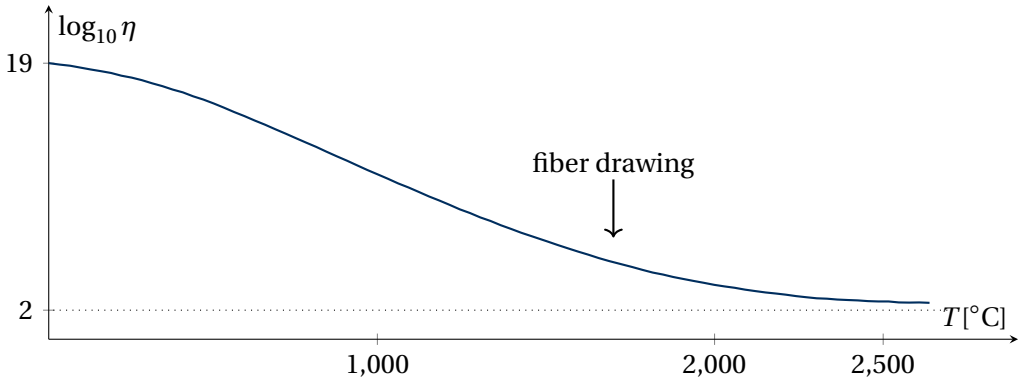

Figure 30: Viscosity of fused silica as a function of temperature.

We can summarize the different regimes of viscosity in the following table:

η[dPa s]	Regime	Analogue
10^{19}	Glass at room temperature	solid
10^{13}	Transform temperature	solid
$10^{7.6}$	softening point	lava
10^{5}	flow temperature	Tar
10^{4}	working point	Ketchup
10^{3}	melting point	Olive oil

Fiber Drawing

The idea is to use a large preform of glass, local heat it and then pull the glass into a long fiber. The regime for this fiber drawing lies between 10^4 to 10^5 dPa s. The schematic of a fiber drawing facility is shown in figure 31.

If we assume that the volume of the fiber and preform are conserved in the time interval Δt, the volume of both parts can be written as

$$\left.\begin{array}{ll} \text{preform} & V_P = A_P v_P \Delta t \\ \text{fiber} & V_F = A_F v_F \Delta t \end{array}\right\} V_P = V_F \quad \Rightarrow \quad d_P^2 v_P = d_F^2 v_F. \tag{3.26}$$

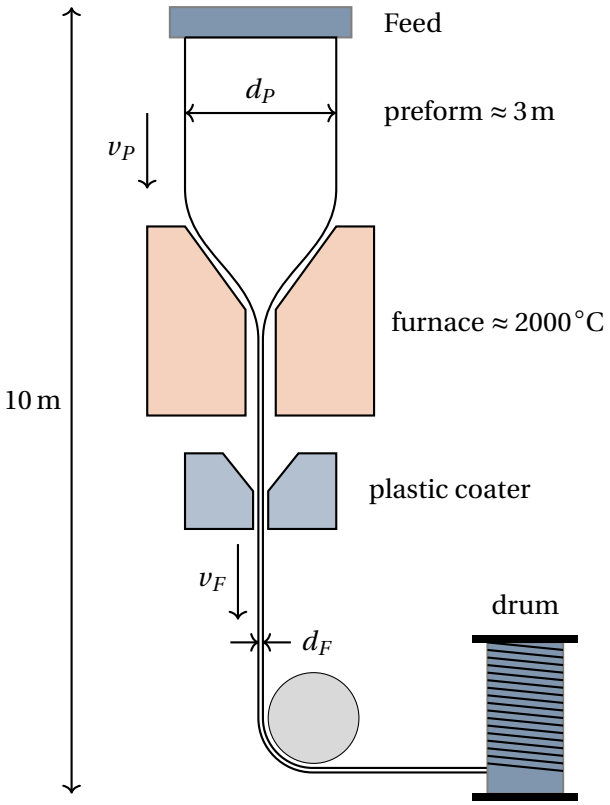

Figure 31: Schematic of a fiber drawing facility. A three metre long preform is heated in an oven and then drawn into a thin fiber of diameter d_F, coated with a plastic and than wound up onto a drum. The polymer coating serves a dual purpose, as it provides mechanical protection and preserves the transmission properties of the fiber. The fiber diameter is monitored optically by diffracting light emitted by a laser from the fiber.

We can rearrange this to find a result for the diameter of the fiber

$$d_F = \sqrt{\frac{v_P}{v_F}} d_P, \tag{3.27}$$

therefore the fiber dimensions can be controlled via the drawing conditions. A higher drawing speed of the fiber results in a thinner diameter. For example, with the fiber parameters $d_F = 128\,\mu\text{m}$, $d_P = 10\,\text{cm}$, $v_P = 0{,}1\,\frac{\text{mm}}{\text{s}}$ we would find a drawing speed of

$$v_F = \left(\frac{d_P}{d_F}\right)^2 v_P \approx 60\,\frac{\text{m}}{\text{s}}. \tag{3.28}$$

Preform fabrication

There are two main techniques to produce preforms. We start with the *gas-phase deposition* (only for silica fibers). With this technique we can produce really high quality fibers because gases can be purified much better than solid or liquids. We distinguish between two approaches:

We only discuss the most import technique, the MCVD. This process is used for almost all GeO_2-doped fibers and consits of two steps depicted in figure 32.

Inside tube	Outside tube
Modified Chemical vapor deposition (MCVD)	Outside vapor deposition (OVD)
Plasma chemical vapor deposition (PCVD)	Plasma outside vapor depos.(POVD)

The fabrication of preforms with the MCVD process is very flexible since the combination of more than one dopant is possible. A desired index profile can be fabricated by simply varying the flow rate from layer to layer. In the related process (PCVD), the chemical reaction is initiated by a microwave plasma. In contrast, in the OVD and POVD method the core and cladding layers are deposited on the outside.

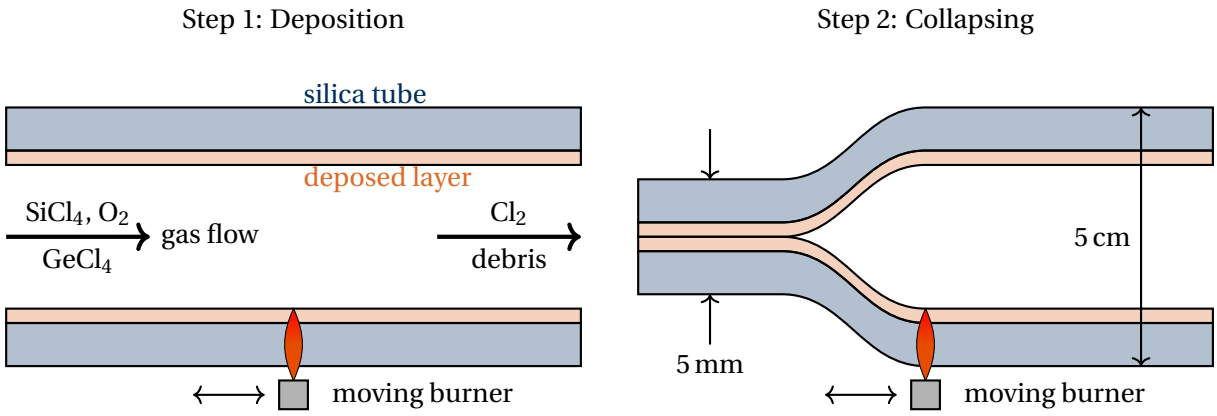

Figure 32: Step 1: In this process, successive layers of SiO_2 are deposited on the inside of a fused silica tube by maxing the vapors of $SiCl_4$ and O_2 at a high temperature of 1800 °C. A moving burner is moved back and forth across the tube using a translation state. When a sufficient cladding thickness has been deposited, the core is formed by adding $GeCl_4$. This reacts with oxygen for form GeO_2. Note that the whole apparatus is rotating.
Step 2: When all layers forming the core have been deposited the burner temperature is raised to collapse the tube into a solid rod.

The second technique we want to discuss is *Stack-And-Draw*. It relies on stacking together silica tudes and rods of a typical length of one metre. During the drawing, the

$$\frac{d}{\Lambda} \quad \text{ratio is conserved.} \tag{3.29}$$

In fact, the ratio is a key parameter in preform fabrication. The Stack-And-Draw method is a flexible technique to realize sophisticated fibers as shown in figure 34.

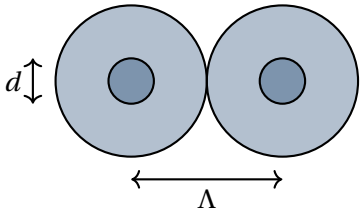

Figure 33: Definition of Λ, d.

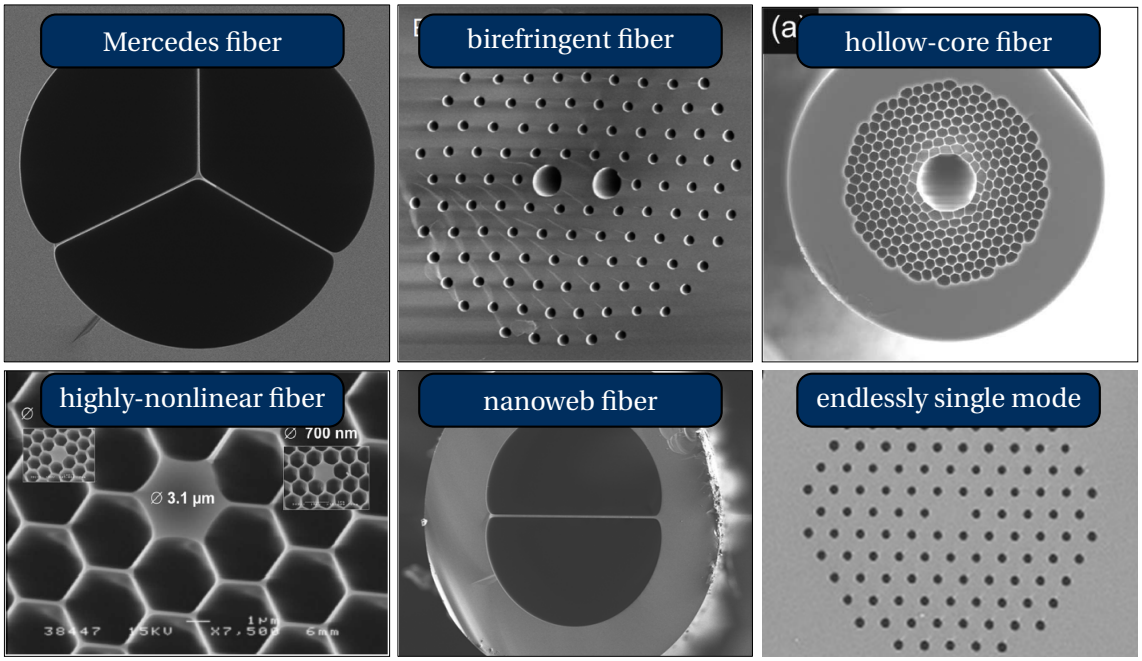

Figure 34: Fibers made by the Stack-And-Draw technique.

4 Types of Fibers

4.1 Circular fibers

Circular fibers are the most import type of fibers because they can be drawn in a simple procedure as described in the previous chapter. Many circular fibers have a small refractive index contrast in the order of 10^-3. This allows us to use the weak guidance approximation which leads to the formation of LP-modes. Let us discuss the two basic configurations of circular fibers shown in figure 35.

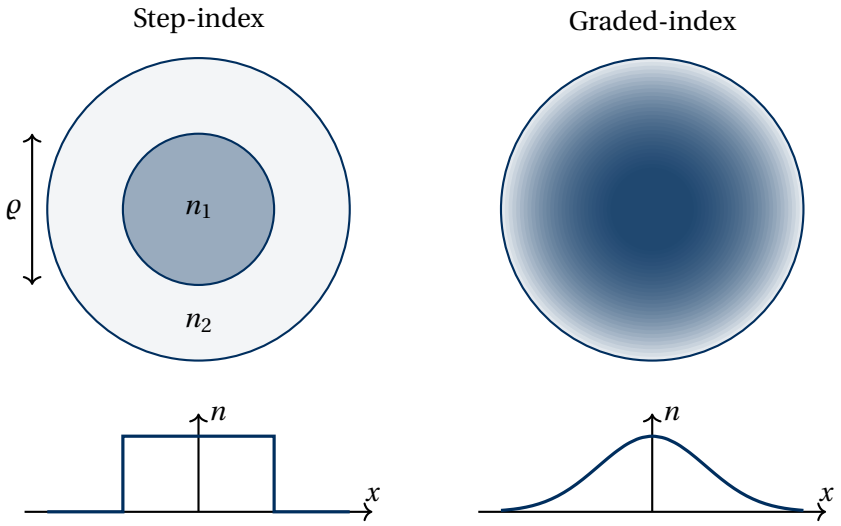

Figure 35: Two basic configurations of circular fibers: Step-index and Graded-index fiber with a continuously varying refractive index.

For step-index fibers we can define a so called *profile height parameter* defined as

$$\Delta = \frac{1}{2}\left(1 - \left(\frac{n_2}{n_1}\right)^2\right) = \frac{n_1^2 - n_2^2}{2n_1^2} \ll 1, \tag{4.1}$$

which is small for small refractive index contrast. Furthermore we want to define the *infinite power-law profile*

$$n^2(R) = \begin{cases} n_1^2(1 - 2\Delta R^q) & 0 \le R < 1 \\ n_1^2(1 - 2\Delta R) = n_2^2 & 1 < R < \infty \end{cases}, \quad \text{with} \quad 0 < q < \infty, R = \frac{r}{\varrho}. \tag{4.2}$$

The parameter q allows to characterize the refractive index profile. Let us display the refractive index profile for various values of q as shown in figure 36.

It can be shown that for $\mathrm{LP}_l m$-modes with $l = 0$, under the assumption of large V-parameters, the following equation holds:

$$U = \left[Q(2m+1) \cdot V^{2/q}\right]^{\frac{q}{q+2}} \quad \text{with} \quad Q = \frac{\Gamma\left(\frac{1}{q} + \frac{1}{2}\right)(q+2)\sqrt{\pi}}{2\Gamma\left(\frac{1}{q}\right)}, \tag{4.3}$$

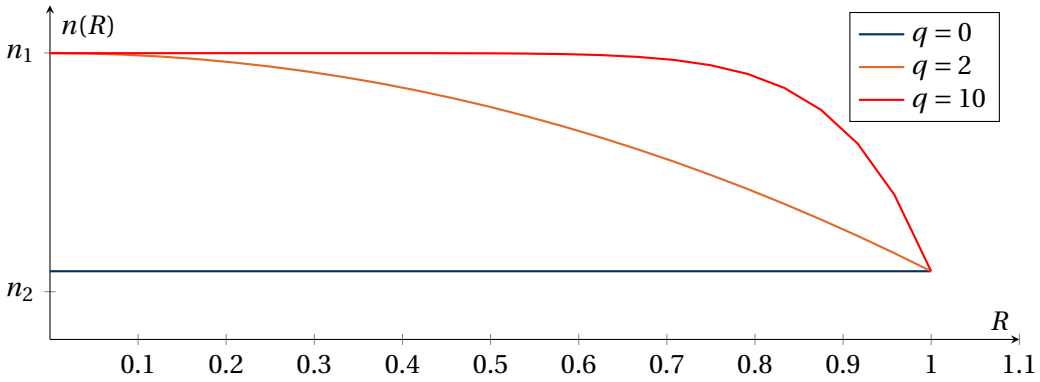

Figure 36: Graphical depiction of the infinite power law profile. For $q = 0$ we have a uniform medium. For $q = 2$ we can model a parabolic profile. In the limiting case of $q \to \infty$ we can model a step-index fiber.

where Γ is the Euler-Gamma function. From the definition of the modal parameter $U = \varrho\sqrt{k_0^2 n_1^2 - \beta^2}$ (equation (2.34)) we find an analytical equation for the dispersion of the infinite power profile

$$\beta = \frac{1}{\varrho}\sqrt{k_0^2 n_1^2 \varrho^2 - \left[(2m+1)QV^{2/q}\right]^{\frac{q}{q+2}}}. \tag{4.4}$$

4.2 Step-index profile

For the step-index profile we have $q = \infty$ with a refractive index

$$n^2(R) = \begin{cases} n_1^2 & 0 \le R \le 1 \\ n_2^2 & 1 < R < \infty. \end{cases} \tag{4.5}$$

4.2.1 Single-Mode fiber

The Single-Mode fiber was already described in great detail in chapter 2. We have seen that there is no real analytic expression of the propagation constant. The most widely used Single-Mode fiber is SMF-28 with the following parameters:

- Core: GeO_2-doped silica, Cladding: Fused Silica
- Manufacturer: Corning (US)
- Core/cladding refractive index difference: $n_1 - n_2 = 5 \cdot 10^{-3}$
- Core Diameter: 8,2 µm
- Attenuation:
  - $\gamma = 0{,}32\,\text{dB/km}$ at $\lambda_0 = 1{,}31\,\mu\text{m}$ (zero dispersion wavelength)
  - $\gamma = 0{,}18\,\text{dB/km}$ at $\lambda_0 = 1{,}55\,\mu\text{m}$

- Higher-Order-Mode cut-off wavelength: $\lambda_{\text{cut}} = 1{,}26\,\mu\text{m}$
- Group velocity dispersion: $D < 18\,\frac{\text{ps}}{\text{nm km}}$ at $\lambda_0 = 1{,}55\,\mu\text{m}$
- Dispersion parameter: $V = \frac{2\pi\varrho}{\lambda_0}\sqrt{n_1^2 - n_2^2} = 2.4068$ Single-Mode

4.2.2 Multi-Mode-Fibers

Typically Multi-Mode-Fibers also have a very small refractive index contrast $\Delta \ll 1$. Furthermore the radius of the core is much larger than the wavelength $\varrho \gg \lambda_0$ which leads to large V-parameters. For a step-index fiber ($q \to \infty$) we again find LP_{0m}-Modes with an effective index

$$n_{\text{eff}} = \frac{1}{4\varrho}\sqrt{16 n_1^2 \varrho^2 - (2m-1)^2 \lambda_0^2}. \tag{4.6}$$

For the fundamental mode ($m = 1$) we have

$$n_{\text{eff}}^{\text{FM}} = \frac{1}{4\varrho}\sqrt{16 n_1^2 \varrho^2 - \lambda_0^2}. \tag{4.7}$$

Let us consider the following example of $n_1 = 1.45$, $n_2 = 1.44$, $\varrho = 100\,\mu\text{m}$ shown in figure 37.

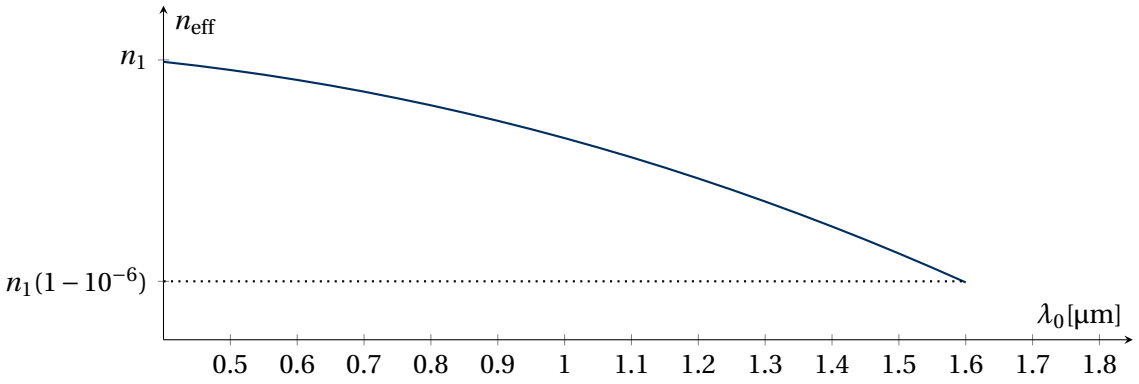

Figure 37: Effective index of a Multi-Mode-fiber of core diameter $\varrho = 100\,\mu\text{m}$. Note that the change of effective index is in the order of 10^{-6}.

Let us calculate the waveguide parameter at $\lambda_0 = 1{,}55\,\mu\text{m}$ which is $V = 34.35$. The number of modes is now given by (2.63)

$$M = \frac{4V^2}{\pi^2} + 2 \approx 2000. \tag{4.8}$$

Therefore this is considered a highly Multi-Mode fiber.

4.3 Parabolic profile fibers

In this case we have $q = 2$ and the refractive index distribution is

$$n^2(R) = \begin{cases} n_1^2(1-2\Delta R^2) & 0 \le R \le 1 \\ n_2^2(1-2\Delta R) & 1 < R < \infty. \end{cases} \tag{4.9}$$

We also assume a small index profile ($\Delta \ll 1$) and a large core radius $\varrho \gg \lambda_0$ (large V-parameter). Since for a parabolic index distribution the core diameter is no well defined quantity we rather determine it as a fitting parameter by fitting the parabolic profile to the measured index distribution. The effective index is then given as

$$n_{\text{eff}} = \frac{1}{2\pi\varrho}\sqrt{4n_1^2\pi^2\varrho^2 + 2(1-2m)V\lambda^2}. \tag{4.10}$$

Let us again consider the example from the step-index fiber with $n_1 = 1.45, n_2 = 1.44, \varrho = 100\,\mu\text{m}$ shown in figure 38.

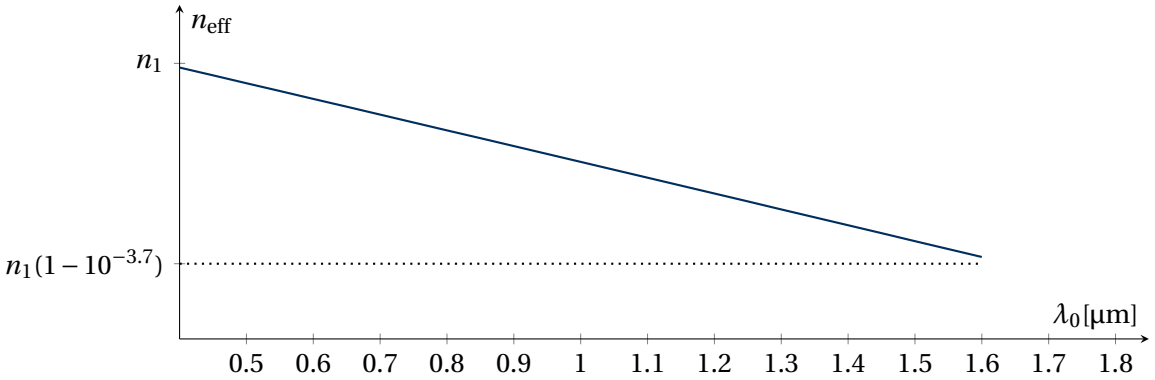

Figure 38: Effective index of a Multi-Mode-fiber of core diameter $\varrho = 100\,\mu\text{m}$ for a parabolic profile. Note that the change of effective index is much higher as for the step-index fiber. Als the curve looks linear, since the argument of the $\sqrt{\dots}$ in (4.10) depends only linearly on λ (note that $V \sim 1/\lambda$).

Let us now compare the group velocity of different Multi-Mode fibers

$$\begin{aligned} \text{Step-index: } v_g^{\text{MMF}} &= \frac{c_0}{4n_1^2\varrho}\sqrt{16n_1^2\varrho^2 - (2m-1)\lambda^2} \\ \text{Parabolic: } v_g^{\text{MMF}} &= \frac{c_0}{n_1^2\varrho}\sqrt{n_1^2\varrho^2 - \frac{(2m-1)V\lambda^2}{2\pi^2}}. \end{aligned} \tag{4.11}$$

We can compare both expressions as a function of the mode number in figure 39. Since Multi-Mode fibers are most commonly used for image transportation, it is desirable that the group velocity of all modes is the same. Therefore, for these kinds of applications, the parabolic profile fiber is used.

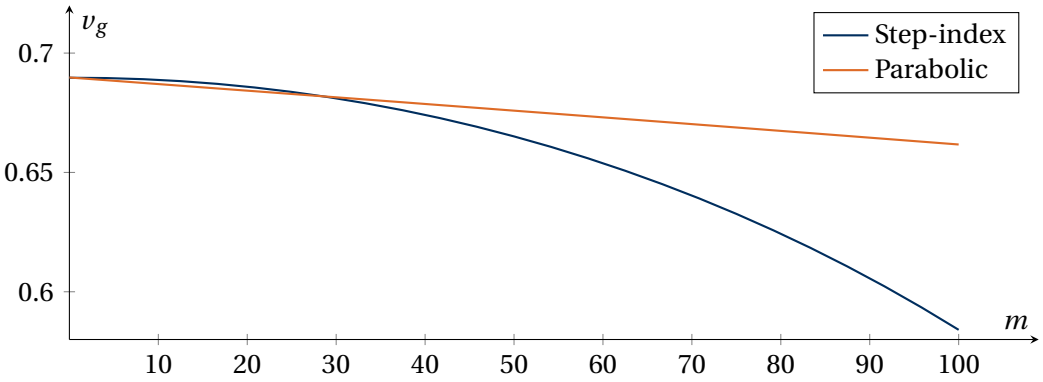

Figure 39: Comparison of the group velocity of Multi-Mode-fibers of core diameter $\varrho = 100\,\mu m$ for a step-index and parabolic profile as a function of the mode number m. For the parabolic fiber, the group velocity changes linearly for increasing mode number, thus exhibits less dispersion (smaller group delay difference) than the step-index fiber.

4.4 Microstructured Optical Fibers (MOF)

The classification of MOFs relies on the refractive index distribution. Via an averaging of the refractive index we can model the MOF as a step index fiber as indicated in figure 40.

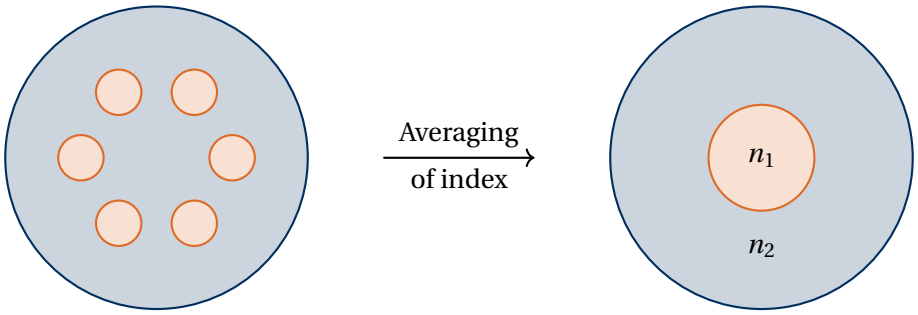

Figure 40: Averaging of refractive index in a Microstructured fiber. n_1 and n_2 are the average indices in core and cladding respectively.

We can now distinguish two different types of MOFs, based on whether $n_1 > n_2$ or vice versa. This is shown in table 3.

Table 3: Two different classifications of MOFs.

	Type of guidance	Examples	Supported mode
$n_1 > n_2$	Total internal reflection	Suspended Core Fiber Endlessly SMF	Guided
$n_1 < n_2$	Photonic Band Gap Effect Low density of States Anti-Resonant Reflection	PBG-Fiber, Omniguide, Kagome-Fiber Negative-Curvature Fiber	Leaky

4.4.1 MOFs with high index core

We first start to discuss MOFs which fulfill the guidance condition we already discussed before $n_1 > n_2$. Many of these MOFs use a solid core and a microstructured cladding. This leads to a modified total internal reflection.

Suspended Core Fibers (SCF)

Suspended Core Fibers have very large air holes near the core region. We can model this fiber as a cylindrical step index fiber with a glass core and an effective cladding medium having the refractive indices

$$n_1 = n_{\text{glass}}, \quad n_2 = n_{\text{glass}} f + n_{\text{air}}(1-f), \tag{4.12}$$

with a filling factor f in the range $0 \leq f \leq 1$.

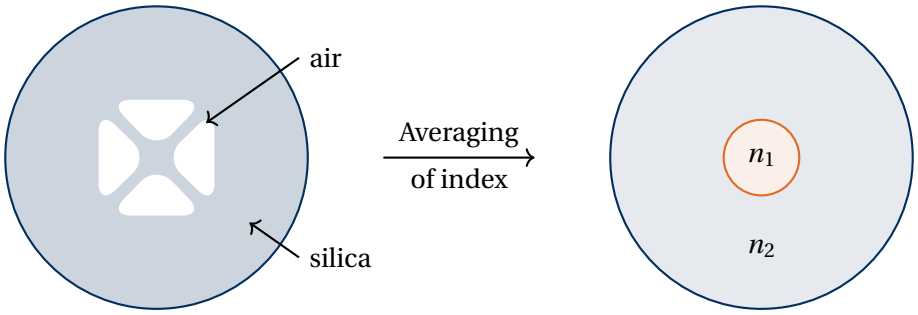

Figure 41: Transverse profile of a Suspended Core Fiber. We can model the structure with a glass core n_1 and an effective cladding medium n_2.

The large air holes are useful to introduce liquids into the fiber. This can be used for sensing or plasmonics. Furthermore by changing the filling factor we can create a tunable cladding index. This can be used for nonlinear light generation (supercontinuum generation, soliton formation).

Endlessly Single Mode Fiber

The special feature of this WG is that in case that the d/Λ ratio is

$$\frac{d}{\Lambda} < 0.4 \quad \text{Endless-Single-Mode} \quad , \tag{4.13}$$

the fiber is Single-Mode for all wavelengths. We want to discuss the physical origin of this pheonomenon. Basically the array of strands acts as a modal "sieve", where all higher order modes can escape the array of air holes. For a qualitative description we define the *transverse wavelength* $\lambda^{\perp}$ using the transverse wave vector $k_{\perp}$

$$n_1^2 k_0^2 = \beta_j^2 + k_{\perp}^2 \quad \Rightarrow \quad k_{\perp} = \sqrt{n_1^2 k_0^2 - \beta_j^2} = \frac{2\pi}{\lambda_j^{\perp}}. \tag{4.14}$$

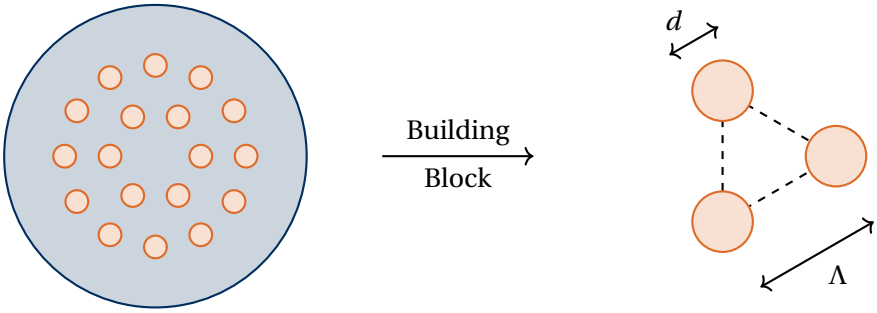

Figure 42: Transverse profile of the Endlessly Single-Mode Fiber.

Then, using $n_{\text{eff}} = \beta_j / k_0$ we find

$$\lambda_j^{\perp} = \frac{\lambda_0}{\sqrt{n_1^2 - n_{\text{eff,j}}^2}}. \tag{4.15}$$

We can plot this as a function of the effective index as shown in figure 43. Since the fundamental mode has a higher effective index than the higher order modes (c. f. figure 11) we can conclude

$$n_{\text{eff},1} > n_{\text{eff},2} \Rightarrow \lambda_1^{\perp} > \lambda_2^{\perp}, \tag{4.16}$$

meaning that higher-order modes have a shorter transverse wavelength. Then, if the fiber is designed correctly, the fundamental mode cannot *squeeze* through two adjacent air-holes, but higher-order modes can.

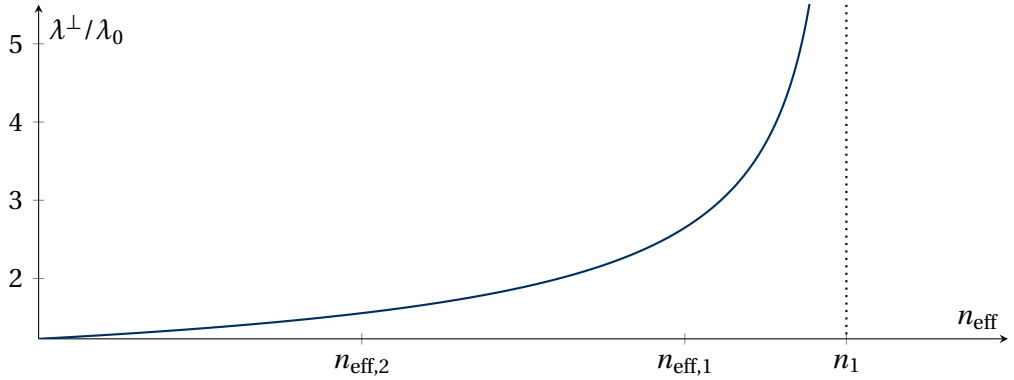

Figure 43: Transverse wavelength as a function of the effective index for $\lambda_0 = 1\,\mu\text{m}$ and $n_1 = 1.45$.

Endlessly SMF can be used for the generation of nonlinear light and broadband light transport.

4.4.2 MOFs with low-index core

A low core index means, that we cannot utilize the effect of total internal reflection. Modes in these fibers will continuously dissipate energy along the transverse direction. This leads to the description of *leaky modes*. The microstructure is then introduced to reduce the loss in longitudinal direction.

Table 4: Comparison of the two index configurations of MOFs. Note that the attenuation for the leaky modes depends on the cladding microstructure.

Configuration	Type of Mode	n_{eff}	Reflect.	Transm.	Attenuation
$n_1 > n_2$	Guided Mode	$n_2 < n_{\text{eff}} < n_1$	1	0	None
$n_1 < n_2$	Leaky Mode	$\text{Re}(n_{\text{eff}}) < n_1$	< 1	> 0	Yes

All leaky modes have complex effective index n_{eff} even if all materials involved are lossless (dispersionless).

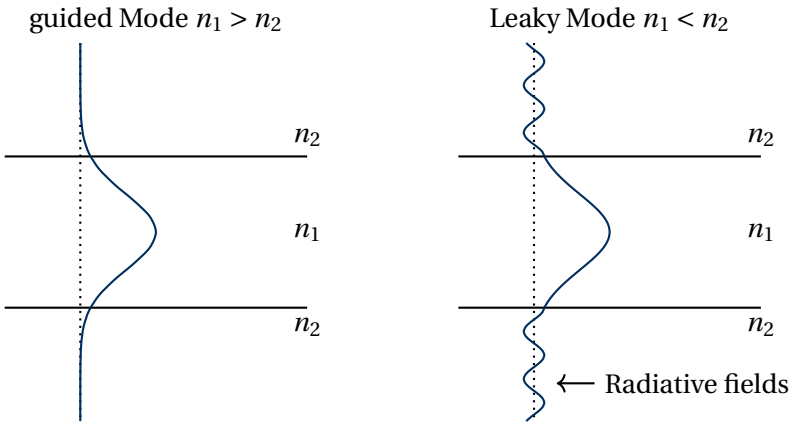

Figure 44: While the fields of the guided modes have evanescent fields in the cladding, while the leaky modes have radiative fields where energy dissipation takes place.

The simples cylindrical leaky waveguide is the *capillary* which only consists of an air core and an infinitely extended cladding made of fused silica. To solve this problem in detail we could use the dispersion equations derived in chapter 2. However, we omit the calculations, since they are rather extensive and involve complex root finding. In case of $\varrho \gg \lambda$ and $n_1 = 1$ we can consider a simple model called the *Marcantilli model* which describes the losses of this capillary. We define the *propagation length* L_p as the length, where the power has dropped to 1/e of its original value

$$L_P \approx \left(\frac{2\pi}{z_{0,1}}\right)^2 \frac{\varrho^3}{\lambda^2} \frac{\sqrt{n^2+1}}{n^2-1}, \tag{4.17}$$

where $z_{0,1}$ is the first zero of the first Bessel function $J_0(x)$. We plot the propagation length as a function of the core radius in figure 45. We can see that large core diameters allow to propagate over lengths of meters.

The problem with capillary fibers is that they are very bend sensitive. Therefore they need to be kept straight. An application is the nonlinear light generation.

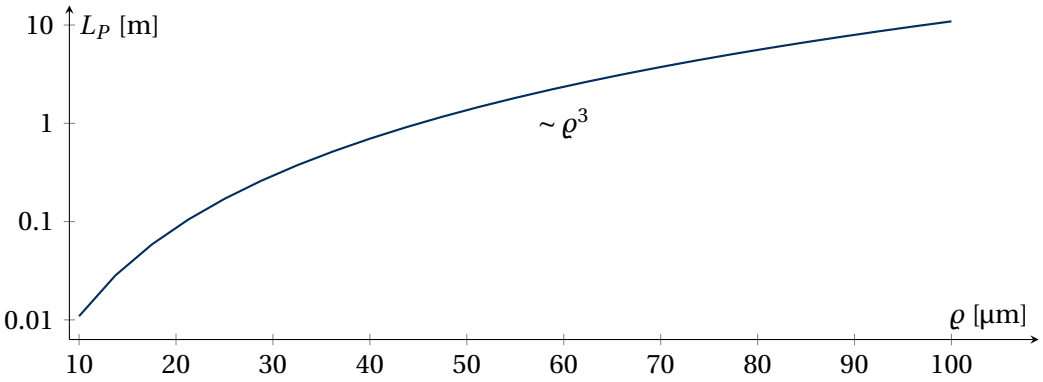

Figure 45: Logarithmic plot of the propagation length of the fundamental capillary mode with $n = 1.45$, $\lambda_0 = 1\,\mu\text{m}$.

Anti-resonant hollow core fiber (ARHCF)

In the following we want to discuss different strategies to design microstructure claddings to reduce modal attenuation. We start with the Anti-Resonant hollow core fibere. The idea is to exploit interference to reduce the attenuation per bounce. This can be done in the simplest way with a thin glass ring as shown in figure 46.

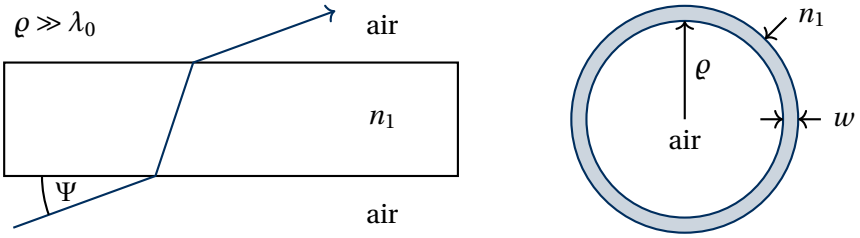

Figure 46: Left: Geometry of the problem. A ray is impinging into the cladding surface with an angle ψ with respect to the cladding plane and is transmitted throug the glass.
Right: Geometry of thing glass ring.

The transmission of a thin slab can be calculated by the coherent sum of the different paths a ray can take to leave the slab on the outside. This is highly dependent on the wavelength as shown in figure 47. The interference can be used to highly reduce the loss.

This effect can be described by the *Zeisberger/Schmidt* model which applies for the fundamental leaky mode. It was developed to describe the dispersion properties of the thin glass ring hollow core fiber. In this model the real part of the effective index is given by

$$\text{Re}(n_{\text{eff}}) = \underbrace{1 - \frac{z_{0,1}^2}{2k_0^2\varrho^2}}_{\text{perfect metal tube WG}} \underbrace{- \frac{z_{0,1}^2}{k_0^2\varrho^3} \frac{\cot\phi}{\sqrt{n_1^2-1}} \frac{n_1^2+1}{2}}_{\text{Induced by resonance}}, \tag{4.18}$$

where $z_{0,1}$ is again the first zero of the Bessel function J_0. Furthermore we can also write down the attenuation coefficient

$$\alpha = \frac{1+\cot^2\phi}{n_1^2-1} \frac{z_{0,1}^3}{k_0^3\varrho^4} \frac{n_1^4+1}{2} \quad \text{with the Phase} \quad \phi = k_0 w \sqrt{n_1^2-1}. \tag{4.19}$$

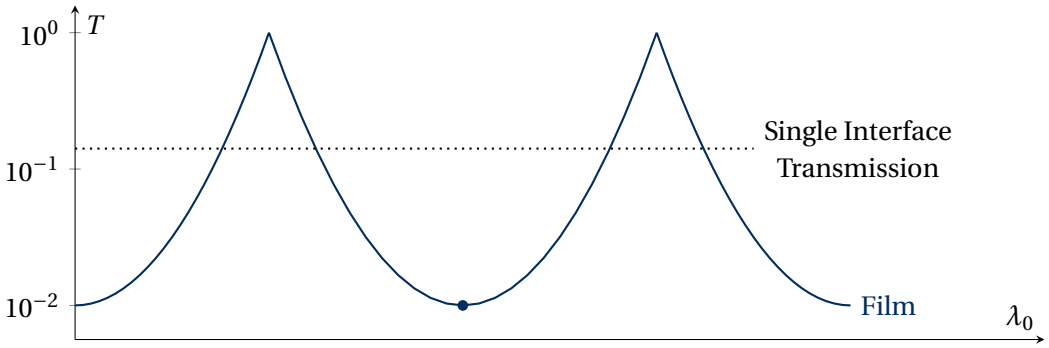

Figure 47: Transmission of a thin slab of glass $n = 1.45$ for grazing incidence rays $\Psi = 1°$. The point of lowest transmission is called the Anti-Resonance point.

Here w is the width of the glass ring as indicated in figure 47. Since the attenuation coefficient is dependent on the cotangent of the phase, it will strongly depend on the wavelength.

At the Anti-Resonant point we have

$$\phi = (2l-1)\frac{\pi}{2}, \quad l = 0,1,2,\ldots \quad \Rightarrow \cot\phi = 0. \tag{4.20}$$

Then the attenuation at this point is given as

$$\alpha = \frac{z_{0,1}^3}{2k_0^3\varrho^4}\frac{n_1^4+1}{n_1^2-1} \quad \Rightarrow \quad L_P = \frac{1}{\alpha} = \frac{2k_0^3\varrho^4}{z_{0,1}^3}\frac{n_1^2-1}{n_1^4+1}. \tag{4.21}$$

In contrast to the capillary WG, the propagation length L_P is now proportional to ϱ^4. Both fibers are compared in figure 48

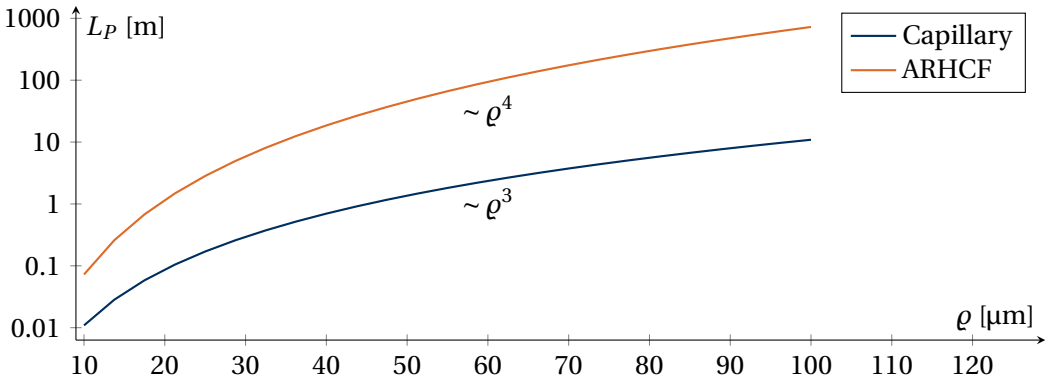

Figure 48: Logarithmic plot of the propagation length of the fundamental capillary mode and fundamental ARHCF-Mode with $n = 1.45$, $\lambda_0 = 1\,\mu m$.

Note that, now for these types of fibers the attenuation is not only dependent on material properties but also on the geometry and structure of the fiber $L_P = L_P(\varrho)$. A much larger core diameter can reduce the loss significantly. In the future, the development of new hollow core fibers can lead to fibers with attenuation may go below the loss limit of typical step-index fibers.

We now introduce the *attenuation improvement factor* as

$$K(\varrho) = \frac{L_P^{\text{ARHCF}}}{L_P^{\text{CAP}}} = \frac{4\pi\varrho}{\lambda_0 z_{0,1}} \frac{(n^2-1)^2}{\sqrt{n^2+1}(n^4+1)}. \tag{4.22}$$

Some typical values are $K(10\,\mu\text{m}) \approx 500, K(100\,\mu\text{m}) \approx 1500$.

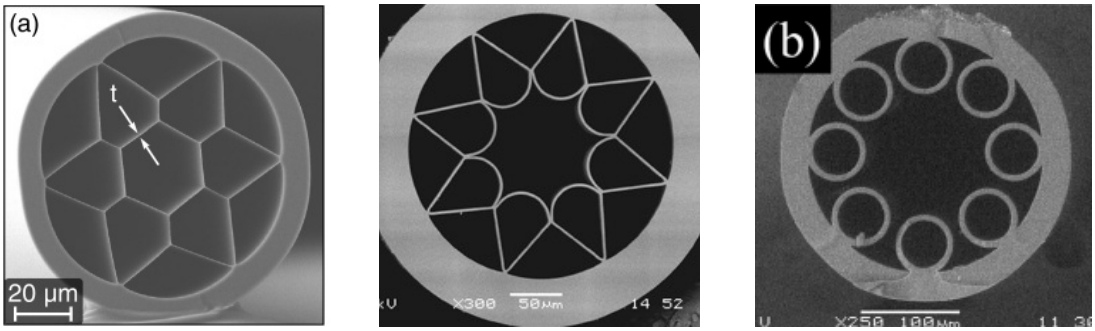

Figure 49: Examples of Anti-Resonant Hollow Core Fibers.
a) This one was produced in Jena at the Institute of Photonic Technology (IPHT). Each structure of the core is surrounded by a ring-type element.
c) Revolver fiber. This recent development seems to beat the loss limit of the solid fibers currently used by telecommunication.

Omniguide

Here the light is confined in the core section via a dielectric multilayer. Then the cladding acts as a Bragg mirror.

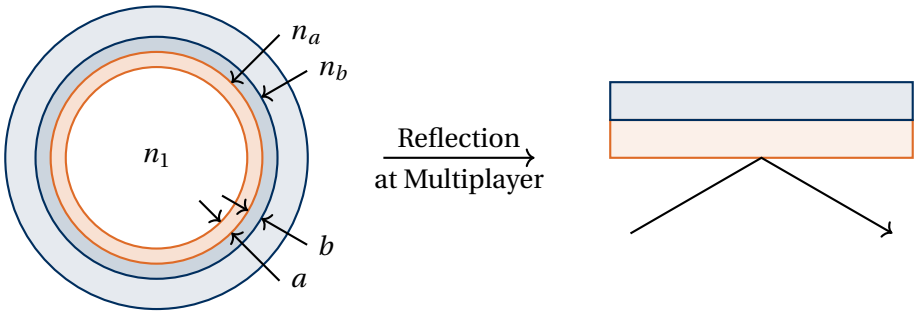

Figure 50: Transverse profile of an Omniguide.

We want to discuss the reflection at a multilayer for normal incidence. At the point of highest reflection, the quarter-wave condition applies. The reflectivity for N double layers of refractive indices n_a and n_b is given by

$$R_N = |r_N|^2 = \frac{C}{C + \left(\frac{\sinh(x)}{\sinh(N\cdot x)}\right)^2} \quad \text{with} \quad x = 2\frac{n_b - n_a}{n_b + n_a} = 2r_{ba} \quad \text{and} \quad C = \frac{|r_{ba}|^2}{1-|r_{ba}|^2}. \tag{4.23}$$

We can plot the reflectivity as a function of the number of multilayers shown in figure 51.

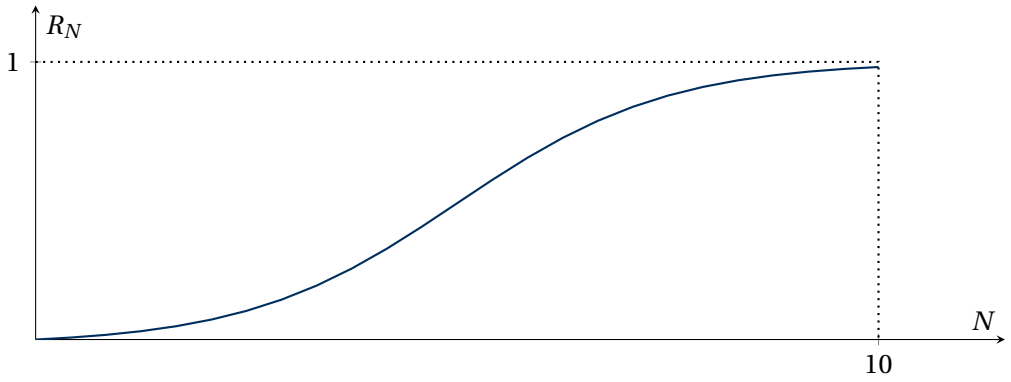

Figure 51: Qualitative plot of reflectivity of a multilayer as a function of the number of double layers N with $n_a = 1.5$ and $n_b = 2.5$.

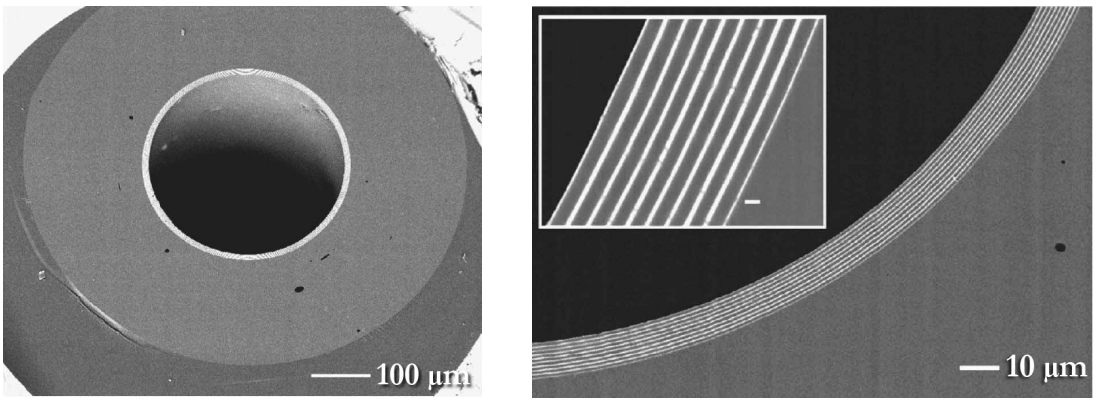

Figure 52: SEM image of an omniguide. Here we can see the multilayer structure consisting of polymer and chalcogenide glass. This particular example of omniguide is used for surgery because it can support high power of CO_2 laser light.

Such a fiber requires a large refractive index contrast which can be implemented via materials like polymers ($n = 1.55$) and chalcogenide glass ($n = 2.5$). Figure 52 shows a Scanning Electron Microscope image of an omniguide fiber.

Finally we want to mention some applications of Hollow core fibers:

- Nonlinear Optics: Strong light-matter interactions in the fiber geometry.
- High power delivery: The very small overlap ($10^{-4} \ldots 10^{-5}$) of the field with the material is useful to couple high power into the fiber.
- Particle guidance: Optical trapping of nano-particles in the fiber.
- Spectroscopy: A large light-matter interaction length is useful for absorption spectroscopy.

Final remark: Hollow core fibers have the potential to break the loss limit of the SMF-28 of 0,16 dB/km (which was already achieved in the visible region).